Review Article

Suresh Sagadevan*, Muhammad Mehmood Shahid, Zhan Yiqiang, Won-Chun Oh*, Tetsuo Soga, Jayasingh Anita Lett, Solhe F. Alshahateet, Is Fatimah, Ahmed Waqar, Suriati Paiman, and Mohd Rafie Johan

# Functionalized graphene-based nanocomposites for smart optoelectronic applications

https://doi.org/10.1515/ntrev-2021-0043
received April 14, 2021; accepted June 14, 2021

**Abstract:** The recent increase in the use of graphene and its derivatives is due to their exceptional physicochemical, electrical, mechanical, and thermal properties as the industrial materials developed by involving graphene structures can fulfill future needs. In that view, the potential use of these graphene-containing nanomaterials in electronics applications has encouraged in-depth exploration of the electronic, conducting, and other functional properties. The protecting undifferentiated form of graphene has similarly been proposed for various applications, for example, as supercapacitors, photovoltaic and transparent conductors, touch screen points, optical limiters, optical frequency converters, and terahertz devices. The hybrid composite nanomaterials that undergo stimulus-induced optical and electrical changes are important for many new technologies based on switchable devices. As a two-dimensional smart electronic material, graphene has received widespread attention, and with that view, we aim to cover the various types of graphene oxide (GO)-based composites, linking their optical and electrical properties with their structural and morphological ones. We believe that the topics covered in this review can shed light on the development of high-yield GO-containing electronic materials, which can be fabricated as the field moves forward and makes more significant advances in smart optoelectronic devices.

**Keywords:** graphene oxide, optical properties of graphene oxide, graphene synthesis, functionalized graphene, optoelectronic devices

## 1 Introduction

Graphene is exciting as the gateway to a new era in materials science and technology research because of its ability to convert itself into many different forms with a change of structure and dimensionality. Figure 1 shows the schematic representation of many different shapes of graphene and their formation. The very supportive, flexible, and film-forming morphology of graphene allows for their wrapping, rolling, and can even be staking into zero-dimensional (0D) fullerenes, one-dimensional (1D) carbon nanotubes (CNTs), two-dimensional (2D) graphene, or three-dimensional (3D) graphite, as shown in Figure 1 [1,2]. The graphene with its 2D carbon sheet maintains several other magical properties such as the thickness similar to that of a single-atom, large theoretical surface area, high conductivity at room temperature, and wider electrochemical window [3]. In addition to those magical properties, the graphene nanosheets (NSs) can also serve as an excellent host material for the growth of high-performance nanomaterials with enhanced electrochemical characteristics [4–7]. Such enhancing electrochemical characteristics, in particular, have the conductivity properties to significantly

* **Corresponding author: Suresh Sagadevan,** Nanotechnology & Catalysis Research Centre, University of Malaya, Kuala Lumpur 50603, Malaysia, e-mail: drsureshnano@gmail.com
* **Corresponding author: Won-Chun Oh,** Department of Advanced Materials Science and Engineering, Hanseo University, Seosan-Si, Chungnam 356-706, Republic of Korea, e-mail: wc_oh@hanseo.ac.kr
**Muhammad Mehmood Shahid, Zhan Yiqiang:** Center of Micro-Nano System, School of Information Science and Technology, Fudan University, Shanghai, 200433, China
**Tetsuo Soga:** Department of Electrical and Mechanical Engineering, Nagoya Institute of Technology, Gokiso-Cho, Showa-Ku, Nagoya 466-8555, Japan
**Jayasingh Anita Lett:** Department of Physics, Sathyabama Institute of Science and Technology, Chennai 600119, Tamil Nadu, India
**Solhe F. Alshahateet:** Department of Chemistry, Mutah University, P.O. Box 7, Mutah 61710, Karak, Jordan
**Is Fatimah:** Chemistry Department, Universitas Islam Indonesia, Kampus Terpadu UII, Jl. Kaliurang Km 14, Sleman, Yogyakarta 55584, Indonesia
**Ahmed Waqar:** Institute of Advance Studies, University of Malaya, Kuala Lumpur 50603, Malaysia
**Suriati Paiman:** Department of Physics, Faculty of Science, Universiti Putra Malaysia, 43400, Serdang, Selangor, Malaysia
**Mohd Rafie Johan:** Nanotechnology & Catalysis Research Centre, University of Malaya, Kuala Lumpur 50603, Malaysia

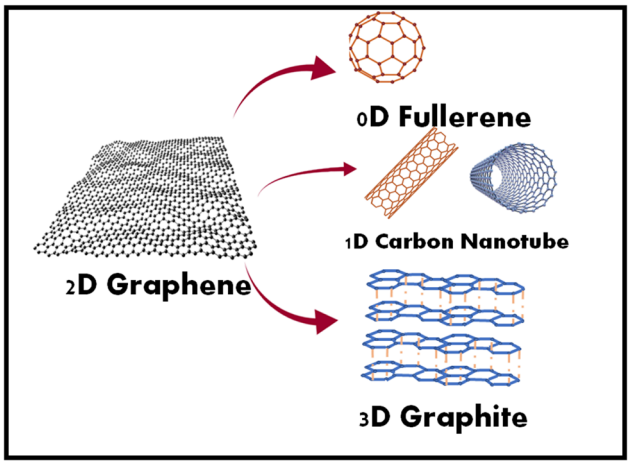


**Figure 1:** (a,b) Graphene is a 2D building material with its wrapped (0D Buckyball's), rolled (1D nanotubes), and stacked (3D graphite) forms.

affect the sensitivity due to the high surface area and dense analyte molecules [8–11].

In comparison to the CNTs, the graphene material not only possesses similarly stable physical properties but also is cheaper to produce along with the maintenance of more edges that particularly helps for the tuning of edge structure, especially the functional groups [12].

Graphene has the properties of the theoretical specific surface area of 2,630 $m^2 g^{-1}$, high intrinsic mobility of 200,000 $cm^2 V^{-1} s^{-1}$, high Young's modulus ~1.0 TPa, thermal conductivity ~5,000 $Wm^{-1} K^{-1}$, optical transmittance ~97.7%, excellent biocompatibility, and super-paramagnetism, which can expand its applications to several fields [13,14]. The common applications include field-effect transistors, functional devices (signal emission, transmission, modulation, and detection), sensors and metrology, transparent conductive films (TCFs; can reach up to 97.7% in the near-infrared and visible region), clean energy devices (graphene-based electrodes for lithium-ion batteries [LiBs] and electrochemical double-layer capacitors), biomedical applications, optical electronics, composite materials, catalysis (oxygen reduction reaction), and photovoltaic cells [12,13,15–24].

The origin of graphene was started 8 years after the award of the Nobel prize in physics and 14 years since the first report of monolayer graphene [25,26], where the researchers' attention to graphene-based magical composites continued to the boom. The main attraction of graphene is the cross-functionality of 2D atomic crystals with unique characteristics, and at the same time, 2D structure sometimes creates hurdles in the exploitation using its zero-gap semi-metal property. To overcome such limitations of graphene, it can be transformed into distinctive forms, such as quantum dots (QDs), nanoribbons, foams, and hydrogels according to suitability [18,27–30].

Graphene is the parent of all graphitic forms of carbon and is a monolayer of carbon atoms joined collectively by a foundation of protruding $sp^2$ hybrid bonds [31]. The exceptional properties of graphene are derived from the 2p orbitals of π-state bands; as a result, the graphene inherits various characteristics, such as being optically transparent and having better surface area, excellent thermal conductivity, and mechanical properties [32]. These characteristics furnish graphene with a significant dominance over similar materials used in diverse industrial applications. Attributable to this, there is always a rising demand for high-quality graphene in vast quantities from both academia and industry to meet these increasing requirements and propel the material into commercial domains. Since graphene's discovery, it has revolutionized the field of nanotechnology because of its single-layered one-atom-thick flatbed structure [33]. Up until now, many attempts have been made to synthesize graphene at a large scale to fulfill the industrial demands, in particular for industries that use graphene to produce state-of-the-art composite materials; hence graphene changed the global market dramatically. Since the discovery of graphene in 2004, it has stormed the field of nanotechnology with an exponential increase in its applications as it appears as a "magic bullet" on the horizon of the composite world. The research related to graphene and graphene-based nanocomposites has generated many reports and that is why Geim says that graphene research has reached unexpected heights in the area of materials science [34].

Some of the pioneering research in the area of graphene/graphene oxide (GO) includes reduced graphene oxide (rGO)–cobalt oxide ($Co_3O_4$)@Pt nanocomposites for nitric-oxide sensors [10], GO–Ag nanocomposites for the detection of nitrite ions [35], $Co_3O_4$ nanocube-doped ChGP nanocomposites for methylene blue dye degradation [36], rGO–$Co_3O_4$ nanocubes as an anode material for the direct methanol fuel cell [5], and rGO/$Co_3O_4$ nanocomposites for supercapacitor applications [37]. The discovery of 0D buckminsterfullerene [38], and shortly thereafter 1D CNTs [39], has increased the interest of research in carbon-based nanomaterials [40]. It is proposed that fullerenes and CNTs are the derivatives of 2D graphene sheets, which are viewed as the chief building block material for all other allotropes of carbon (Figure 1). Similarly, graphite is made up of stacked sheets of graphene one on another maintaining the interlayer distance (3.37 Å) [41]. Also, a section of graphene sheet can be

virtually wrapped or rolled to make "fullerenes" and "CNTs" [42], but in reality, they are not derived from graphene. For the lab-scale production of graphene, numerous methods have been devised. These include the "scotch-tape method" as the primary one [33] that can be adopted for the isolation of pure defect-free graphene, followed by numerous other synthesis processes such as exfoliation methods [43–47], chemical vapor deposition (CVD) [44–49], pyrolysis [49], chemical synthesis [50], arc discharge [50], unzipping of CNTs [51], solvothermal [52], epitaxial growth [44], molecular beam epitaxy [53], and electrically assisted synthesis [54]. As shown in Figure 2, the mechanical exfoliation of graphene results in the generation of pristine graphene (pure and unoxidized form) in a bottom-up approach, while the chemical oxidation forms GO and further exfoliation and reduction ultimately produce rGO in a top-down approach [55].

In this review article, we have focused on the recent research including the synthesis and applications of graphene-based nanocomposites. Though the special focus of this article is on graphene and functionalized graphene-based materials for optical applications, it also provides an overview of graphene synthesis (bottom-up and top-down approaches) and its characteristics, since graphene is the main roll material of the current review article.

## 2 Properties of graphene

For the formation of strong covalent bonds, there are three electrons involved per carbon atom of graphene, and one out of the three electrons per atom yields the bonds. The electrons are responsible for the electronic properties at low energies and form energy bands far away from the Fermi energy [56]. Graphene has $sp^2$ hybridization between S and P orbitals, which makes trigonal planar structure by forming a bond between carbon atoms at 1.42 Å distance. The band between carbon atoms strengthens the lattice structure of all allotropes. Out of many interesting properties, graphene has its low-energy excitations massless, chiral, and Dirac fermions; moreover, at a neutral pH, graphene has the chemical potentials that cross exactly the Dirac point. The specific dispersion, which is possible only at low energies, imitates the quantum electrodynamic (QED) physics for massless fermions with only a difference of speed vF of Dirac fermions in graphene, which is 300 times slower than the speed of light. Hence, graphene bears many of the unusual properties of QED at smaller speeds (Figure 3) [57–59]. As shown in Figure 5, graphene's electronic orientation and its structure support for very high charge mobility. Still, for the long term, the mobility of graphene is mostly limited to 2,000–15,000 $cm^2 V^{-1} s^{-1}$ and is because of the defect levels, microscopic ripples, and scattering [33,60,61]. Furthermore, the clean surface-suspended graphene has carried mobility up to the range of 200,000 $cm^2 V^{-1} s^{-1}$, and such suspended graphene can reduce the scattering by making use of the substrate, and due to which the carrier mobility and ballistic transport become possible. This ultrahigh mobility carrier enables new provisions in the field of electronics and optoelectronics [62].

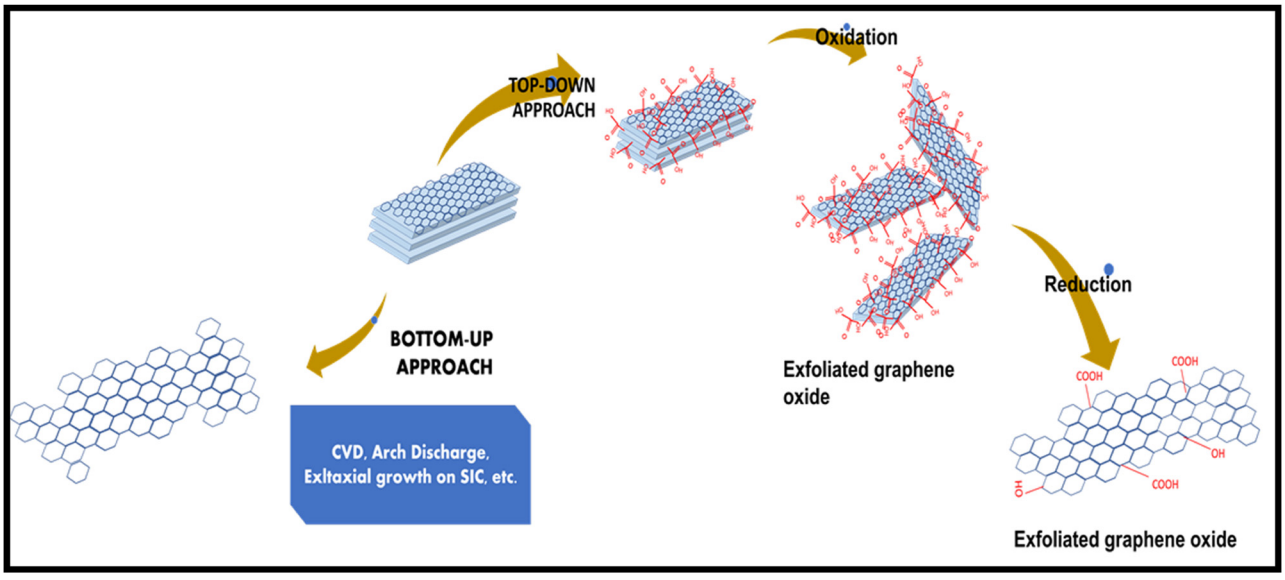


**Figure 2:** Schematic representation of the methods used for the synthesis of graphene, which is classified into top-down and bottom-up approaches.

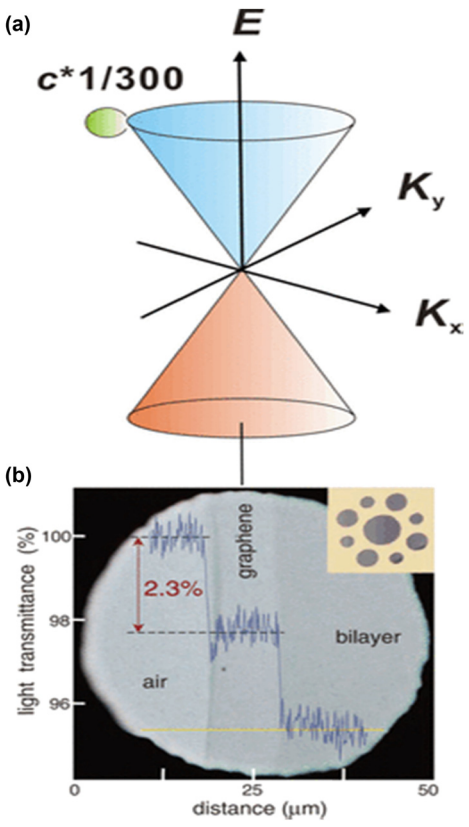


**Figure 3:** (a,b) Electronic and optical properties of graphene; linear energy dispersion of massless Dirac fermions (MDFs) in graphene [63].

## 2.1 Optical properties

Graphene with its multilayer structure can absorb radiation over a range of frequencies, and its ability to generate optical transitions in the electric fields is called gate-dependent optical transitions [64–68]. The absorption rate of mono- and bilayer ability of graphene in the presence of light is shown in Figure 4a, and the graphene material can absorb only 2.3% of its incident white light with 97.7% transmittance [69]. The graphene has the thickness of one atom, and the frequency of incident light has no relationship with the intensity of absorption [26]. These exceptional characteristics result from the electrons, conical band, and holes at the Dirac fermions in its sheets [70]. However, the bilayer graphene can absorb white light up to 4.6% and in accordance with the increase of the number of layers, the absorption capabilities of graphene also increase linearly. The individual layer absorption can be obtained as $A = 1 - T = \pi\alpha = 2.3\%$, where $\alpha$ ~1/37 represents the fine-structure constant [71]. So, with each layer absorbing 2.3% of light and with a graphene sample of five layers can have a total of 11.5% absorption and 88–88.5% optical transparency. Hence in a study, the ultraviolet radiation spectrum in the wavelength range of 900–300 nm was used to identify graphene, where the results proved that the graphene under these conditions is featureless, and at the same time, the maximum absorption was noted for this material around 270 nm wavelength, thereby confirming its optical properties at specific regions [69].

## 2.2 Linear absorption

The unique band structure of graphene has novel optical properties, *i.e.*, when incident light falls on the surface of graphene, the electrons are ejected from the valance band and excited to the conduction band by absorbing the photon energy. Thus, the conductivity caused by photons in single-layer graphene depends upon the structural constant as follows [63]:

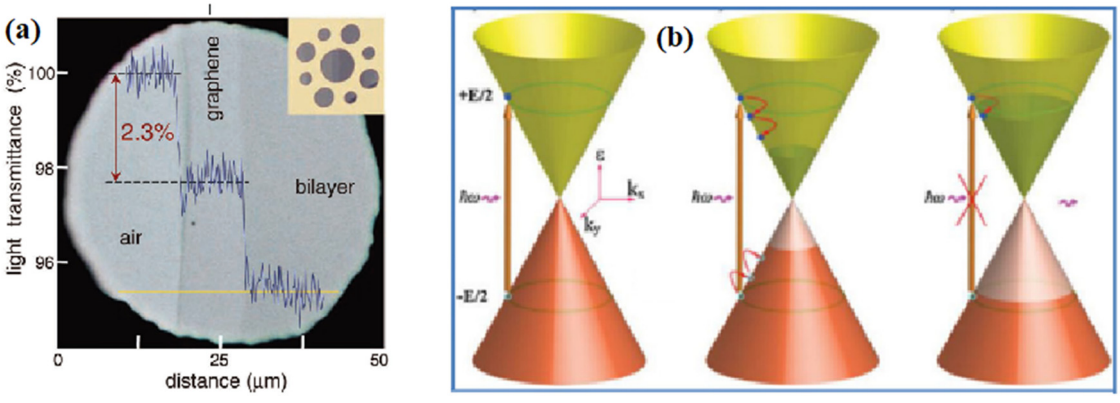


**Figure 4:** (a) Absorption rate of mono- and bilayer graphene in the presence of light and (b) the dynamic simulation of graphene-saturated absorption [73].

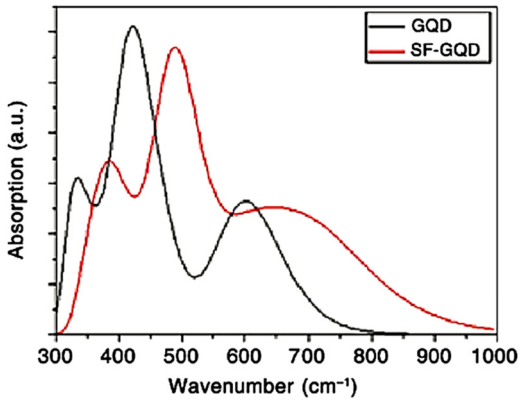


**Figure 5:** Comparison of the UV-Vis absorption spectra of GQDs and surface functionalized GQDs [86].

$$\alpha = e^2/4\pi\varepsilon_0\hbar \approx 1/137. \quad (1)$$

Also, $T$ is the linear transmittance of single-layer graphene and is represented as follows:

$$T = 1/(1 + 0.5\pi\alpha)^2 \approx 1 - \pi\alpha \approx 97.7\%. \quad (2)$$

In the visible region, the reflectance of graphene is less than 0.1% and is counted as 2% for graphene with ten layers. Figure 4b represents the dynamic simulation studies of graphene to explain its optical properties, and from that, it can be inferred that graphene can absorb light of any wavelength due to the zero bandgap [72]. Furthermore, the theoretical calculations also confirm that graphene can absorb different bands of light at different configurations of QDs and substrate-based graphene [49,50]. Graphene maintains its absorption rate of light even at weak incident light power when the energy band near the Dirac point of graphene is not filled. It is observed that graphene cannot continue the absorption of light to achieve sutural absorption because of the Pauli blocking effect. It has a nonlinear absorption [51–56], and its saturable absorption (SA) coefficient can be calculated as follows [51]:

$$\alpha^*(N) = \alpha^* S/(1 + (N/N_S)) + \alpha^* N_S, \quad (3)$$

where $\alpha^* S$ and $\alpha^* N_S$ represent saturated and unsaturated absorption components, respectively, $N$ is the photo-induced electron–hole density, and $N_s$ is the saturation density.

## 2.3 SA

SA is a nonlinear occurrence consisting of the quenching of optical absorption beneath high-intensity radiation. Thus, the outcome of SA is a continuous wave broken down into a train of ultrashort pulses, which are the key constituent of passive-mode locking (PML) in laser cavities. Most of the materials need higher optical intensities even closer to their optical-damage threshold, at which they undergo SA [74]. In this phenomenon, the mirrors used to operate in a narrow spectral range need advanced fabrication methods, since they are not very tunable. Recently, carbon-based nanomaterials have proved themselves to be potential, cost-effective, and feasible alternatives for developing next-generation PML lasers. Graphene, as a carbon material, has played a role in overcoming these limitations with its strange conical band structure [75], giving rise to broadband resonant SA even at remarkably low light intensities [76]. Moreover, graphene's band structure can be further tuned by applying an external voltage to the gate [77]. The PML ultrafast laser action, broadband adjustability, and exchange quality factor are few of the properties that can be accomplished using SA components prepared using graphene to generate large energy pulses. Modern theories have shown that the single-mode function of the random laser is achievable by implanting graphene flakes in the gain medium [78]. For this purpose, the single-particle MDF representation turns out to be a suitable theoretical support [79].

## 2.4 Luminescence

Graphene has been used for photoluminescence and electromagnetic transport applications because of its extraordinary characteristics and so has created a wide range of research interests [80–83]. The fragmented graphene and graphene-derived QDs (GQDs) present exceptional photoluminescence properties in the preparation process and make graphene a photoluminescent material taking advantage of the coherence between π electrons that can be reduced by tuning its chemical and physical properties. The oxidation plasma treatment of single-layer graphene sheets can introduce bright light into it [80], and in the same way, the bulk graphene and dispersion can exhibit a large uniform area of photoluminescence [84,85]. A routinely prepared photoluminescent graphene material can be used in sandwich form with a conductive layer of graphene to make sandwich-type light-emitting diodes (LEDs), which can operate with a wavelength range of infrared to blue [80]. In general, G-QDs are synthesized using a blue-radiated hydrothermal method [83]. Wang and his colleagues investigated the photoluminescence mechanism in G-QDs [86] and found

that the excited-state transfer between electrons and holes and the influence of edge-effect light luminescence (as shown in Figure 5) made in visible photoluminescence devices within the scope of the preparation of a theoretical basis.

With a decrease in the size of the QDs, graphene exhibits quantum confinement and unique edge effects [81–86]. A few other reports presented the photoluminescence of GO as recombination of e–h pairs of localized states of the $sp^2$ cluster [84]. The size or conjugate length of the $sp^2$ cluster is the major part that defines the energy gap between π* and π [87], which is likely to be explained by the edge effect of graphene and the defects related to the oxidation process. Some reports say that photoluminescence in GQDs is the consequence of the radiative recombination of electrons at the graphene edges [88], by a transition in free zigzag sites instead of transition between π* and π as defined previously. However, it doesn't matter which mechanism is used for photoluminescence of GQDs, but it has the same characteristics; the excitation wavelength is responsible for the changes in emission spectrum wavelength. Therefore, the organic fluorescent material has a great influence in developing cheap optoelectronic devices [89].

Although the exact structure of GO is not well-understood, there is a general agreement that the bandgap is influenced by morphology sizes, oxygen coverage densities O/C ratio, surface functionalities, and other factors. As the size of GO NSs grows larger, the number of conjugated aromatic rings increases, lowering bandgap energy. Upon conjugation with different functional groups, such as atomic vacancy, hydroxyl, epoxy, and carboxyl groups, the gap energy of ideal graphene clusters decreases. Based on Gaussian and time-dependent DFT simulations, Chien *et al.* found that these functional groups caused distortions in the aromatic rings and that these disorder-induced localized states caused absorption in the lower energy regions (Figure 6) [90].

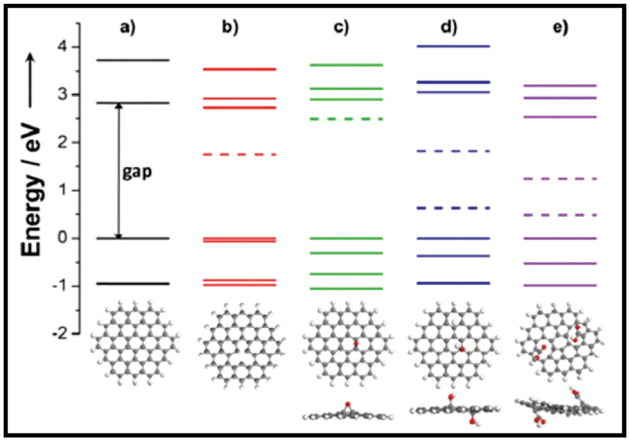


**Figure 6:** (a–e)The energy levels of ideal graphene NSs and decorated with various functional groups, such as atomic vacancy, hydroxyl, epoxy, and carboxyl groups [90].

Thorough investigation of the fluorescence difference between GQDs and graphene-derived GOQDs (GOQDs) will help in the in-depth understanding of their luminescence mechanisms. For example, Liu *et al.* have successfully synthesized highly homogeneous GQDs and GOQDs from the suspension of GO solution after sonication and centrifugation [91]. Both GQDs and GOQDs had circular shapes with a diameter of 4 nm, but GOQDs had different

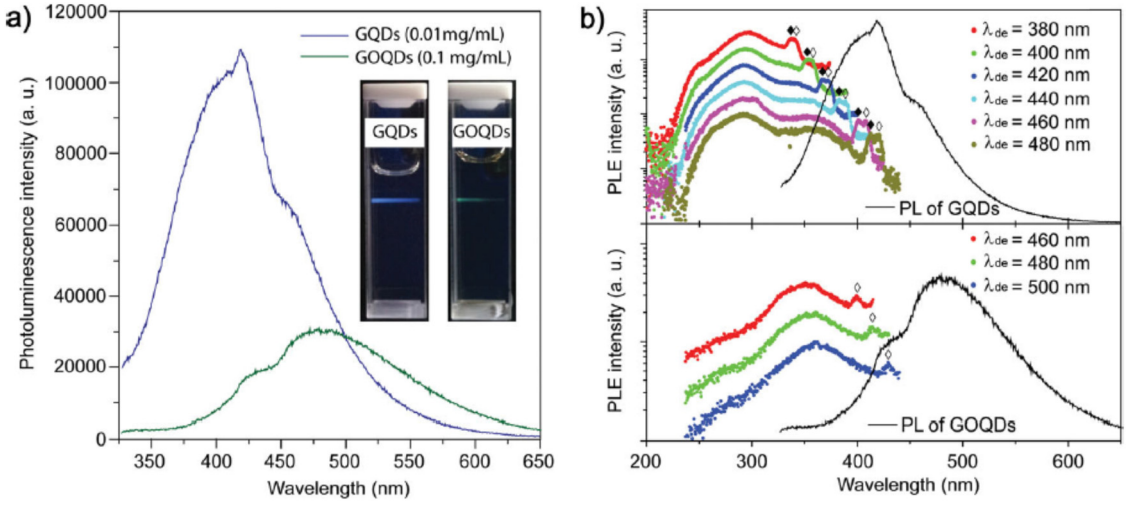


**Figure 7:** (a) PL spectra and the corresponding fluorescent images of GQDs and GOQDs, (b) PL excitation spectra of GQDs and GOQDs with varying detection emission wavelengths [91].

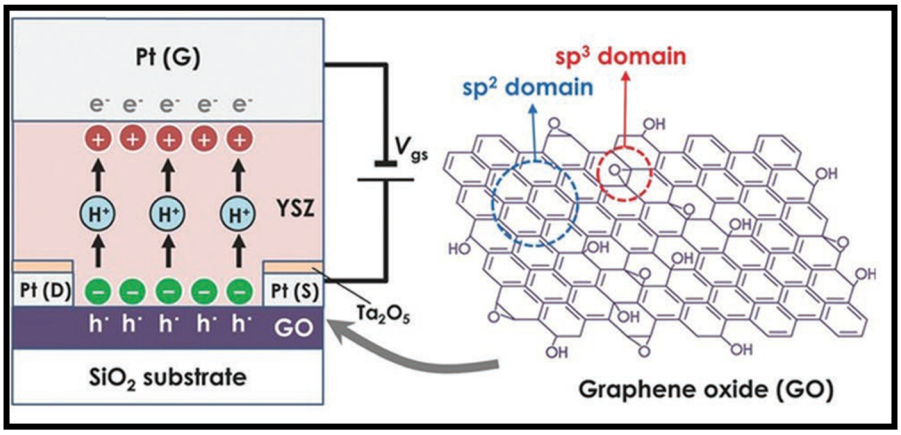


**Figure 8:** Schematic illustration of GO-based all-solid-state electric double-layer transistor. G, S, and D denote the gate, source, and drain electrodes [92].

oxygen-containing functional groups, while GQDs had a pure $sp^2$ carbon crystalline structure without oxygenous defects. GQDs and GOQDs released transparent blue (420 nm) and green color (480 nm) emissions, respectively, according to the spectral analysis, and the fluorescence intensity of GQDs was about 3.5 times higher than that of GOQDs, despite its concentration, which is about 10 times lower (Figure 7a and b) [91].

During the fabrication of graphene from GO NSs, reductive treatment is often used to eliminate oxygen-containing groups. Meanwhile, the bandgap structure of GO NSs is evolving, resulting in a slew of new optical properties. For example, Eda *et al.* observed blue PL based around 390 nm for thin-film samples deposited from thoroughly exfoliated suspensions after exposure to hydrazine vapor [84]. The localization of e–h pairs was facilitated to radiative recombination by adequately regulating the concentration of isolated $sp^2$ clusters within the carbon–oxygen $sp^3$ matrix *via* reduction treatment, and the PL intensity could be increased ten-fold compared to the as-synthesized materials. Furthermore, it was found that the bandgap energy of GO NSs can be continuously tuned by precisely regulating the reductive extent, resulting in a variety of luminescent colors. The bandgap of GO can be *in situ* and nonvolatile tuned by a redox reaction using a solid electrolyte thin film by simply applying direct current (DC) voltage inside an all-solid-state device (Figure 8) [92]. The PL peak wavelength can be adjusted from 393 to 712 nm by changing the applied DC voltage between −3.5 and 2.5 V (Figure 9) [93], where the polarity of voltage was defined as positive when GO was oxidized and negative when reduced. A wide emission peak at 676 nm was observed for pristine GO.

The mechanisms that explain the evolution of GO photoluminescence is shown in Figure 10. Figure 10a shows the original GO, which is made up of various disorder-induced defect states within the p–p* gap and has a large prominent PL spectrum centered at longer wavelengths. As shown in Figure 10b, the number of disorder-induced states within the p–p* gap decreases after deoxygenation, whereas the number of cluster-like states from newly formed small and isolated $sp^2$ domains increases. At shorter wavelengths and with narrower bandwidth, electron–hole recombination among these $sp^2$ cluster-like states induces blue fluorescence. As a result of modifying the heterogeneous electronic structures of GO and rGO with variable $sp^2$ and $sp^3$ hybridizations by reduction, the tunable PL spectra of GO are due to variance of the relative intensity ratios of PL emission from two different forms of electronically excited states [94].

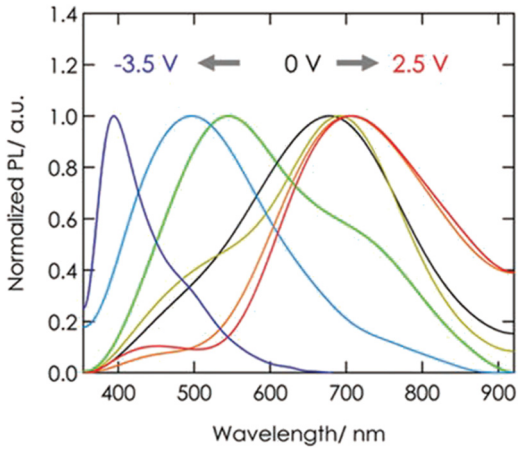


**Figure 9:** DC bias dependence of normalized PL spectra tuned by application of various bias voltages for 1,200 s [93].

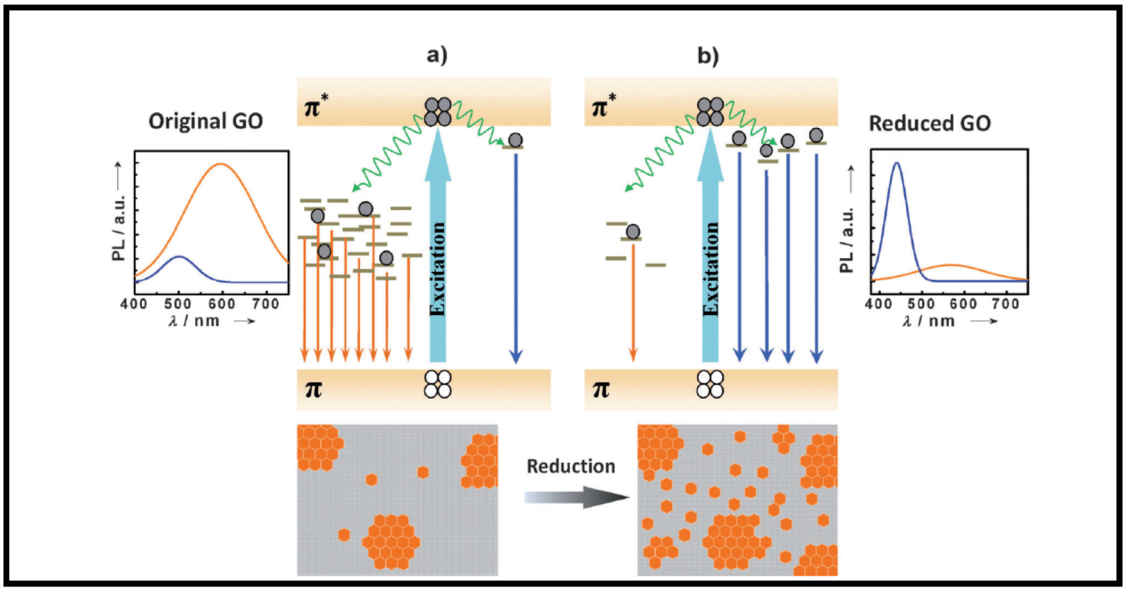


**Figure 10:** Proposed PL emission mechanisms of (a) the predominant IP1 emission in GO from disorder-induced localized states, (b) the predominant IP2 emission in rGO from confined cluster states [94].

# 3 Synthesis approaches of graphene

To synthesize graphene with different outcomes, there are different bottom-up and top-down techniques available. The foremost route used for the synthesis of graphene is direct peeling off graphite using scotch tape, but this option will not work for the commercial production of graphene. The most famous bottom-up route is CVD for the production of a large-area continuous graphene film, and this route comes under the category of bottom-up because it incorporates the simpler molecules to form a continuous graphene film. Moreover, this method takes in hydrocarbon gas as a feeding stock and can result in large-area polycrystalline films that are several square meters in size [95,96]. Even though the CVD method is broadly used, this method has very limited optimal results, because of the defects that endanger the structural capability of thin films to adversely affect their physical properties. Furthermore, because of the lower production rate, this option has no potential for industrial production [48,96,97].

Generally, the top-down approach is used to produce large-scale graphene, starting with graphite to make their flakes by the exfoliation with mechanical, chemical, or electrochemical methods. The two frequently applied methods to form graphene flakes are as follows: (a) oxidation of graphite forming GO, which can be partially deoxidized to produce rGO [98–100], and (b) liquid-phase exfoliation of graphite [101]. In oxidation *via* the Hummers and Offeman method, graphite is generically exposed to a solution of potassium permanganate, sodium nitrate, sulfuric acid, and water. During this process, the carbon scaffold is decorated with 45% of oxygen functional groups (epoxy, carboxyl, and hydroxyl). Since GO is an amorphous material with a higher density of defects because of its intrinsic nature, it can be partially reduced to rGO by removing the oxygen functional groups (about 23%) using different routes. The rGO, with a significant reduction of oxygen contents, performs electrically and thermally better than GO does, but not like graphene, and is still considered to be amorphous [100]. In 2004, Novoselov *et al.* made several attempts to produce a single-layer graphene sheet [33,102,103]. These efforts mainly involve the peeling of graphite crystals with a specific limit using adhesive tape and transferring the thinned-out graphite onto an oxidized silicon wafer with a thickness of <300 nm [102]. This procedure led to the large-scale production of graphene and its application in electronic and polymeric industries. Over many decades, even though there has been a huge difficulty in producing pure, large-scale, and defect-free graphene sheets [55,102,103], the epitaxial growth on metal carbide has become a promising method for the production of graphene [49,102,103].

## 3.1 Top-down approach

As we said, the synthesis of graphene has been widely categorized into “top-down” and “bottom-up” processes.

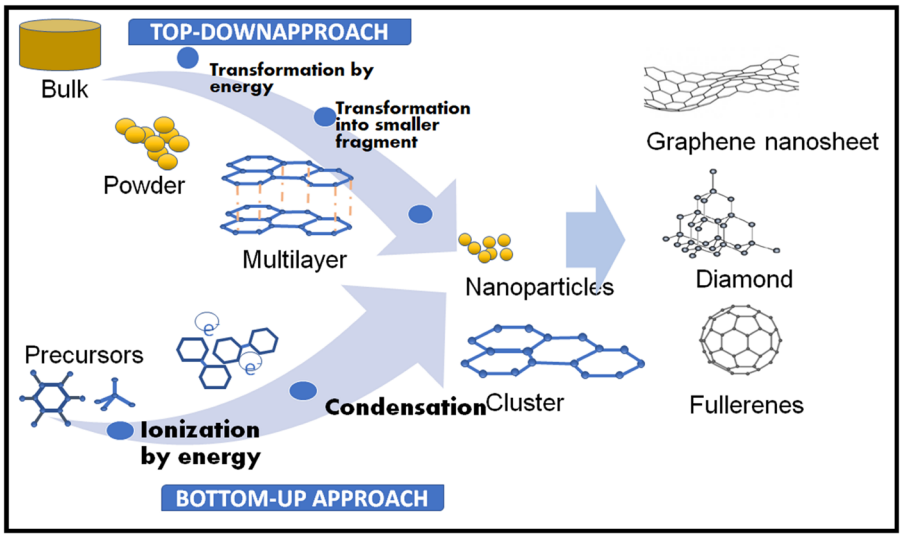


**Figure 11:** Schematic representation of the formation of highly × rGO from graphite using the top-down approach.

The top-down approach is cost-effective and suffers from the limitations of large-scale production and quality control [104]. This approach generally involves the separation, peeling, cleaving, or exfoliation of graphite or its derivatives (GO and graphite fluoride) [105]. Usually, the formulation of imperfection-free graphene with superior quality involves diverse techniques, such as mechanical shedding of graphite, electrochemical peeling, sonication, surface functionalization, acid corrosion disintegration, alkylation of graphene subsidiaries, chemical methods for aqueous/organically treated GO, thermal methods for shedding graphite, and chemical methods for the reduction of GO [55,105]. The production of graphene and its nanocomposites by the peeling, surface functionalization, and chemical reduction with comprehensible strategies has been extensively examined by Potts *et al.* [106]. Comparably, Dhand *et al.* [107] have also investigated the synthesis of graphene, elucidating several analogous approaches. A diagram of the production of graphene by the top-down approach is provided in Figure 11 [108].

A well-thought-out top-down scheme for extricating mono-layered graphene flakes on the preferential substrate is mechanical peeling. This technique is the principally accepted strategy for the synthesis of graphene flakes as it usually necessitates ~300 $nN\,\mu m^{-2}$ force to detach a single atomic layer from graphite's surface. The piling up of sheets in graphite results in some moderately enveloped π orbital, contradictory to the flat surface of the sheet, and the attractive van der Waals force is outstripped with the micromechanical chasm using the scotch tape to separate the graphite sheets [26,103]. A lateral force can also be applied by means of graphite's self-lubricating ability in the lateral direction to promote the relative motion between two graphite layers (Figure 12). These two mechanical routes are considered to be the prerequisites for the production of graphene by exfoliation techniques. Moreover, the tailoring of these two routes could produce high-quality graphene with high efficiency [109]. Although the exfoliation process is a destructive approach, the force generated by exfoliation can also fragment large graphite particles or graphene layers into smaller ones (Figure 12) [110]. This exfoliation reduces the lateral size of graphene, which is not useful for accomplishing large-area graphene or for facilitating the exfoliation into smaller graphite flakes [109].

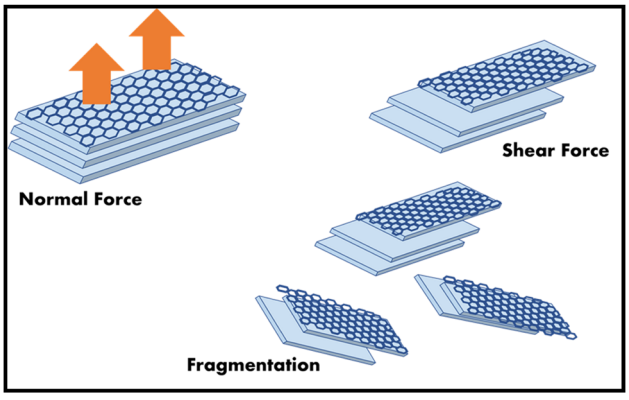


**Figure 12:** Schematic representation of the two kinds of mechanical routes for exfoliating graphite into graphene flakes and the auxiliary route for fragmentation.

### 3.2 Bottom-up approach

The deciding variables for the control of synthesized graphene's morphology, crystallinity, and structure are the tiny molecules of chemicals and catalysts within the bottom-up approach, as in prior discussions [111]. In the literature, the employment of hydrocarbons as a source of graphene has also been reported for the generation and use of metal-ion catalysts in the course of CVD practice [95,111–113]. In the CVD technique, the capability and strength to produce graphene layers are probably tremendous, which makes this technique the most acceptable one for the assembly and manufacturing of devices [111]. The assembling of graphite layers on a silicon–carbide substrate has been used since 1893 [114]. Primarily, Van Bommel *et al.* in 1975 affirmed the growth of graphite on both 6H-SiC (001) substrates [115], and in the recent era, the technique has gained enormous importance because of the high-temperature sublimation escalation deposition of mono-layer epitaxial graphene, grown on the SiC substrate. One group has reported the depositing of mono-layers up to a few layers of graphene deposits on the SiC substrates, mainly by means of high-temperature (1,300–1,800°C) heating of SiC substrate with the use of an ultrahigh vacuum or under an inert atmosphere [114]. As the temperature required for the sublimation of Si is less than that for carbon (~1,500°C), the SiC surface is given a thin layer of carbon [116]. The number of graphene layers stacked and blended onto the SiC substrate depends on the face orientation of the crystal and layer growth conditions. Even though the most commonly used epitaxial graphene growth surfaces are the hexagonal forms of 4H- and 6H-SiC substrates, the CVD graphene growth has been achieved using the cubic 3C-SiC.

In the modern era, the assembly of SiC wafers has become more aggressive because of the demand for epitaxial graphene in the LED industry and in power electronics research. The epitaxial growth is the deposition of a single crystalline film on monocrystalline substrate to facilitate the epitaxial film. Thus, the fabrication involves the deposition of high-crystalline graphene on single-crystalline SiC substrates, either by means of homo-epitaxial (film deposited on the identical substrate) or hetero-epitaxial (film deposited on a dissimilar substrate) growth. In particular, during 2004, the SiC substrates were primarily intended to measure parameters correlated with the electrical measurements because of a wide-bandgap semiconductor (3 eV) on patterned epitaxial graphene [109]. One can anticipate that the epitaxial graphene growth technique on SiC might be an exceptionally good technique for the large-scale assembling and marketing of graphene-accompanied electronics, such as high-frequency electronics, light-emitting devices, and radiation hard devices [117]. Even though the abovementioned technique is very costly, taking into consideration the novel resistance standards located on the quantum Hall effect [118], top-gated transistors have been made up of graphene on SiC [119]. The high-frequency transistors have furthermore been uncovered with a 100 GHz cut-off frequency [120], superior to the state of the art of Si transistors of similar gate length [121].

During the year 2008–2009, the CVD emerged as an outstanding method for the fabrication and assembly of graphene because of its availability, first-rate quality [122], inexpensiveness, and applications involved in the extensive fabrication of flexible crystal-clear conductors for organic photovoltaic (OPV) cells and effectual transistor production [123]. The graphene prepared by the CVD technique is more extensively intended for the fabrication of n-type graphene as compared to the scotch-tape method and can be fashioned in two uncomplicated steps, carbon atoms formed initially as a result of pyrolysis of the precursor material and the disassociation of carbon atoms to shape the carbon structure of graphene. The process is carried out in a high-temperature furnace (1,000°C) in the company of a catalytic agent, where stress is created on the gas-phase surface of the transition-metal substrate (Ni, Cu, Co, Pd, Ir, Au, or Ru) and by exposure to one of the hydrocarbons (methane, ethylene, acetylene, or benzene) to form carbon layers. Furthermore, the furnace is rapidly cooled to keep the precipitated carbon layer from aggregating in order to form bulk graphite in the course of chemical adsorption, thereby crystallizing into a contiguous graphene layer on the metal substrates. Depending on the substrate quality, precursor characteristics, width, and requisite structure, the various types of CVD processes, such as a thermal, plasma-enhanced, cold wall, hot wall, or reactive type CVD, are usually employed [124].

## 4 Functionalization of graphene

Different sorts of materials can be functionalized using graphene to actuate their effectiveness, which incorporates atoms, nanoobjects, and polymers to form electronic or photonic devices, with improved mechanical and thermal properties. Hence, the functionalized graphene nanocomposites can be crafted to attain altogether significantly better performance than that of pure particles, nanoobjects, or polymers.

## 4.1 Functionalization with molecules

One of the conventional and accepted ways to functionalize graphene is by using small molecules; for instance, surfactants, pyridine, protein, DNA, RNA, peptide, and complex compounds, typically the anticancer drugs, can be functionalized on the graphene surface to upgrade and ameliorate the solution dispensation potential, optical, electronic, and bio-related characteristics. Reconstructing the ability of graphene to dissolve in a wide range of solvents is one of the foremost critical purposes of graphene molecular functionalization. The chemically prepared graphene possesses destitute solvency and is exceptionally troublesome to be used in large-scale productions because of the difficulty of handling and complex procedures. As an illustration, sodium dodecylbenzene sulfonate can be functionalized to modify the graphene surface as well as to attain exceedingly soluble graphene over 1 mg $mL^{-1}$ in water, which makes possible solution-based fabrications for the conductive film or any conceivable biological analysis [125–127]. An example of pyridine-based functionalized graphene by Gupta *et al.* is shown in Figure 13 [128].

In order to achieve high solubility, the DNA and protein molecules are used to functionalize graphene as the charges of these biomolecules in the presence of water stabilize the graphene sheets [129,130]. The molecular functionalization improves not only the solubility but also its optical efficiency. A better optical-limiting effect was observed using porphyrin functionalized graphene as compared to the criterion optical-limiting material of C60 [131]. The electron/energy transport that exists between the molecules of porphyrin and graphene was partly responsible for this amazing optical-limiting effect. In another work, the non-covalent bonds and interactions that exist between dendronized perylene bisimides and graphene were accomplished in a homogeneous solution, but the fluorescence of dendronized perylene bisimides was demolished as a result of the above interaction [132]. The characteristics associated with biological molecules tend to be changed by functionalization with graphene. Specifically, the biomolecular functionalization of graphene tends to modify the bio-reactiveness while forming nanohybrids and nanocomposites. For instance, the single-strand DNA forming fusion with graphene has a strong selectivity with the harmonizing DNA down to a single base mismatch [133]. In another work, the non-covalent authoritative and electronic intelligence between dendronized perylene bisimides and

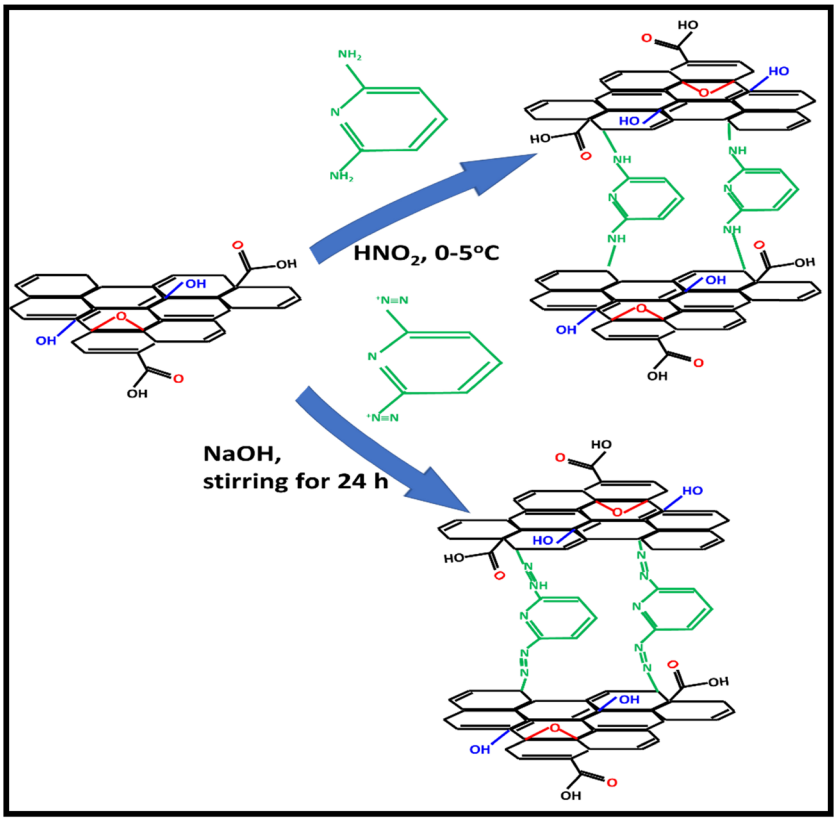


**Figure 13:** Schematic representation of the synthesis of pyridine-based functionalized GOs [128].

graphene was accomplished in a homogeneous arrangement, and the fluorescence of dendronized perylene bisimides was extinguished because of the formation of intelligent-hybrid composite structures [132]. The functionalization of graphene with that of organic molecules and polymers changes the bio-related properties of graphene.

## 4.2 Functionalization with nanoscale objects

The functionalization of graphene heterostructures and nanocomposites with various nanoobjects, such as nanoparticles (NPs), nanowires, nanorods, and NSs, is another kind of functionalization that is often done. Based on the intrinsic properties of materials, the nanoobjects are endowed with various capabilities in contrast to pristine graphene. The nanoobject-based graphene nanocomposites particularly combine specific optical and electronic properties to advance the possibilities of graphene in numerous electronic and optoelectronic operations. Some outstanding optical characteristics are exhibited by the semiconductor nanoobjects that can overcome the low-absorption behavior of pristine graphene. For instance, the semiconductor CdS QDs/NPs have increased the photo-absorption along with photoelectrical responses appreciably when combined with graphene to form nanocomposites [134,135]. Likewise, the ZnO nanowires/nanorod semiconductors that are UV active possess a wider bandgap that can improve the UV response of graphene when combined with graphene/ZnO heterostructures [136]. Likewise, the $TiO_2$ NPs confirmed superior photocatalytic and photoelectrical activity when combined with graphene to form nanocomposites [137]. Furthermore, in electrical and electrochemical aspects, the graphene/nanoobjects exhibit outstanding activity; one study observed that the $MoS_2$ NSs/graphene nanocomposites showcased better electrocatalytic characteristics than did pure $MoS_2$ in a hydrogen evolution reaction [138]. Also, in studies related to electrochemical capacitors, $Ni(OH)_2$, the NSs/graphene nanocomposites confirmed superior performance [139]. Similarly, the $Co_3O_4$ NPs/graphene nanocomposites exhibited much better oxygen reduction than did a C/Pt catalyst, although this activity was scaled down in pure $Co_3O_4$ NPs [140]. The metal NPs, exclusively Pt-functionalized ones with graphene, exhibit an exceptional electrocatalytic activity during methanol oxidization [141]. Figure 14 shows the functionalization of graphene with nanoscale objects by Shahid *et al.* [142].

## 4.3 Functionalization with polymers

An additional functional species extensively used to functionalize graphene is the polymer to produce graphene-based polymer composites. Generally, polymers resembling small molecules have also been functionalized to increase

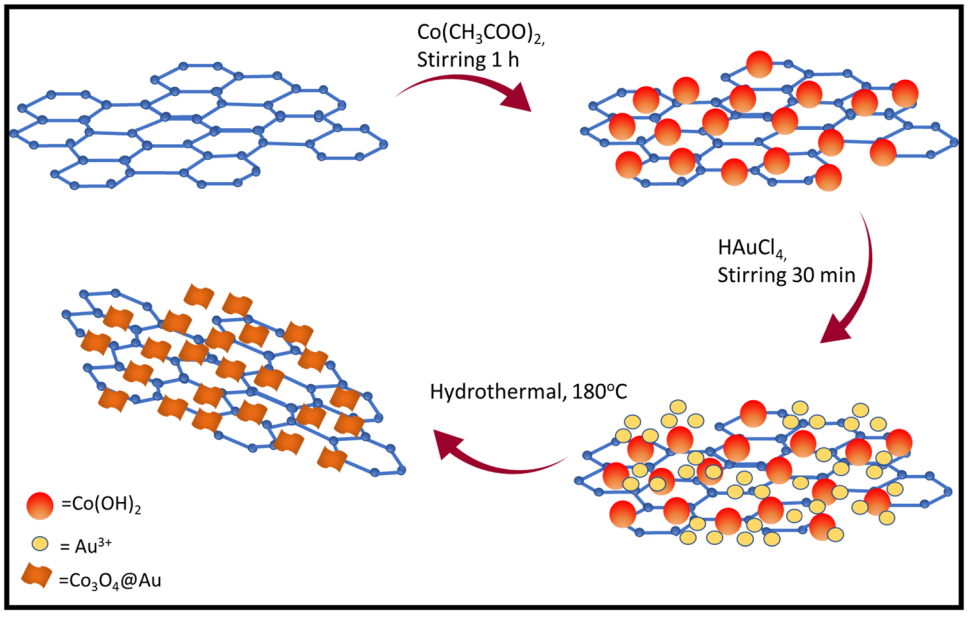


**Figure 14:** A schematic representation of functionalized graphene with $Co_3O_4$ nanocubes and Au NPs.

the solubility of graphene. The amphiphilic conjugated triblock copolymer has been functionalized to increase the solubility of graphene in a variety of organic and inorganic solvents [143]. Sulfonated polyaniline and amine-terminated polystyrene analogous to amine-terminated polymers were initiated to be very successful in enriching the solubility equally in organic solvents and water [144,145]. Exclusively in photonic and ultrafast photonic devices, graphene/polymer nanocomposites have worked well [77,146]. Besides, the optical absorption of the poly(vinyl acetate)/graphene nanocomposites was enlarged ten-fold times using only 0.07 wt% inclusion of graphene [146]. Also, some comparable photonic effects were monitored using polyvinyl alcohol/graphene nanocomposites in mode-locked ultrafast lasers [77]. Similarly, poly(3,4-ethylene dioxythiophene) (PEDOT)/graphene nanocomposites have also increased the photoelectrical activity with an appropriate percentage of graphene in the nanocomposite anode used as the LEDs [147]. Figure 15 shows the functionalization of GO by using functionalization of graphene with polymers [148].

## 5 Photonic and optoelectronic-related applications

In general, to enhance the electron transport mechanism in optically active materials such as ZnO, $TiO_2$, $SnO_2$, *etc.*, the composite formation is the best suitable approach as it can strongly influence the outer electron states and their movement. For example, in a study, Wang *et al.* [149] investigated the optoelectronic properties of $TiO_2$/rGO nanocomposite sheets (with different graphene composition) formed by the hydrothermal method. During the synthesis, the reaction steps to undergo the conversion of graphite into GO first and further to rGO with a 2:1 ratio of water:ethanol blend in the presence of various amounts of tetrabutyl titanate are represented schematically in Figure 16. The investigation exhibited improved nonlinear optical (NLO) characteristics of a $G_{0.25}$ nanocomposite associated with its components, which are endorsed by a blend of mechanisms. The function of defect centers and electron/energy transport in the optical-limiting action of $G_{0.25}$ was verified using Raman and

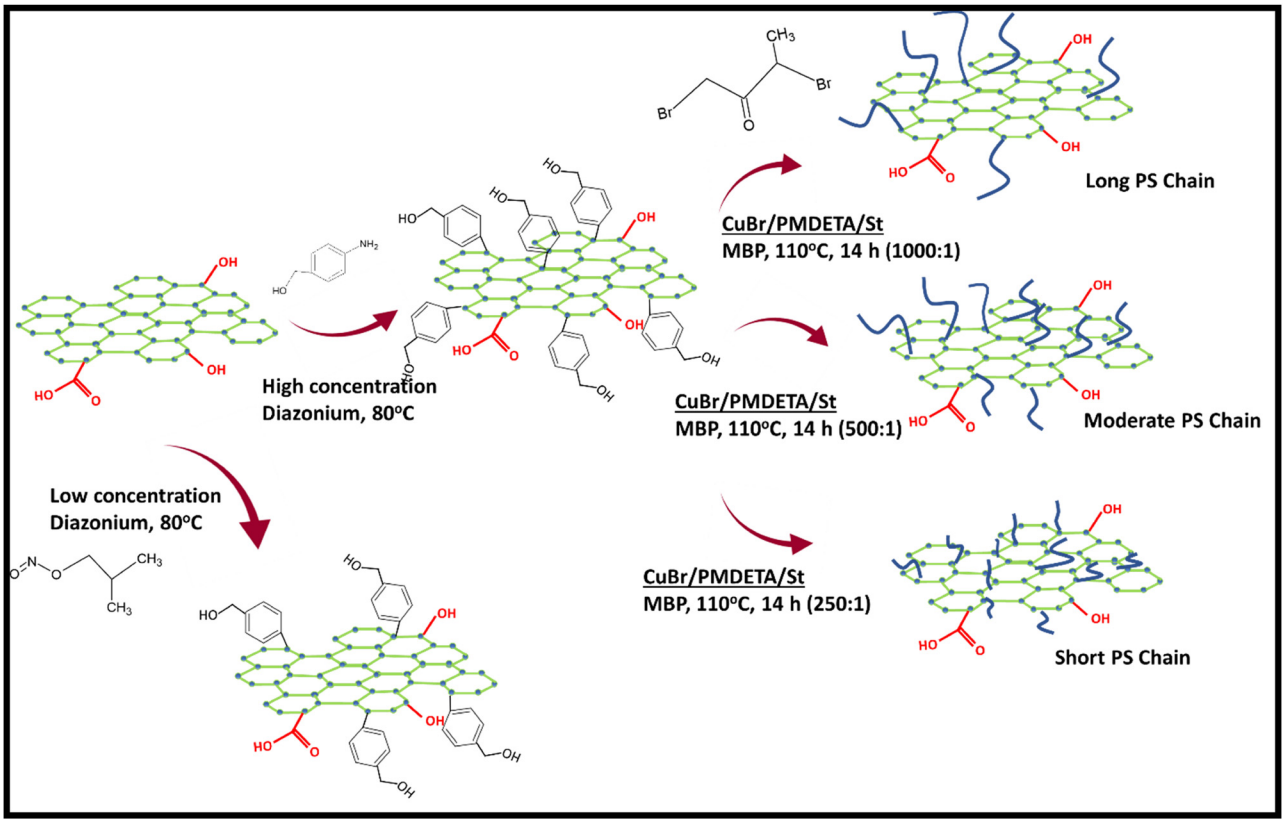


**Figure 15:** Synthetic routes for achieving controllable functionalization of graphene [148].

photoluminescent spectroscopies. Also, the intensity-dependent exchange between reverse saturable and SA actions with $G_{0.50}$ nanocomposite was monitored.

An in-depth analysis reveals that a noteworthy fluorescence quenching has been experienced for all the graphene nanocomposites as compared to $TiO_2$, thereby signifying the occurrence and enhancing of the energy transport mechanism due to the composite formation. To optimize the NLO activity, the NLO absorption characteristics and optical-limiting reactions of nanocomposites were investigated using the Z-scan approach at a wavelength of 532 nm with 4-ns laser pulses using an optimal concentration of $TiO_2$ in nanocomposites. The superior NLO activity was monitored in $G_{0.25}$ nanocomposite, in the nanosecond regime, and can be qualified as a result of the blended NLO mechanism, although the intensity-dependent actions in $G_{0.50}$ were caused by the mutual contribution from ESA and TPA. Overall, these conclusions demonstrate that $TiO_2$/rGO nanocomposites with adequate $TiO_2$ content can provide optical control and NLO switching and thereby theoretically allow the opportunity of ultrafast NLO candidates for photonic and optoelectronic uses.

## 5.1 Photovoltaic cells

Yin *et al.* [141] built transparent and conductive electrodes to be used for flexible OPV appliances (schematically represented in Figure 17) by coating the chemically synthesized rGO over polyethylene terephthalate substrates. The efficiency of OPV appliance chiefly relies on the charge-transport effectiveness when the optical transmittance of rGO is higher than 65% [142]. On the other hand, for lesser transmittance, the efficiency of OPV appliances is controlled by the light-transmission efficiency, *i.e.*, the transparency of rGO films [150]. Following the application of about a 2.9% tensile strain on the fabricated OPV device, the device can sustain for thousands of bending cycles [151], thereby demonstrating for the highly flexible properties of rGO films, and thus indicating the potential applications of these materials toward flexible optoelectronics applications.

A study by Şahin *et al.* [152] synthesized GO using the Tour method and further tailored it with various amine sources (dihexylamine [DHA] and 2-ethylhexylamine [2EHA]) involving various branched alkyl chains. The GOs and modified GOs (mGOs) were used to investigate the efficiency of

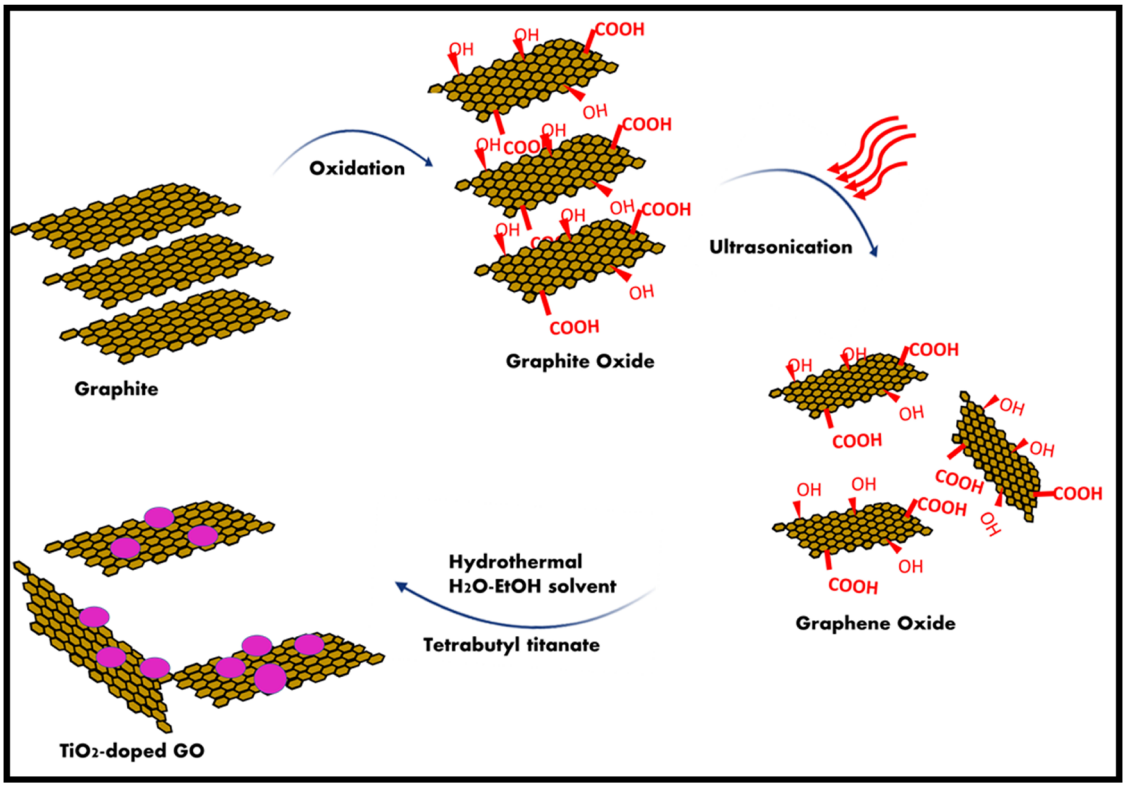


**Figure 16:** Illustration of the fabrication process of $TiO_2$-decorated rGO nanocomposite.

perovskite solar cells by using them as a buffering layer. The mechanism of formation (represented in Figure 18) shows the customized solar cells with the supplementary coating of mGO derivatives sandwiched between the perovskite and hole-transporting film exhibiting the overall efficiency better than that of the reference cell [152]. This improved performance may have resulted from the improved carrier transport *via* the mGOs. To be specific, in general, there was a 10% overall performance boost of the solar cells in solar-cell appliances whenever GO customized with 2EHA was used, as compared to the standard cells used devoid of the modified buffer layer [152].

It can be seen from the investigation that the mGOs, when functionalized as a buffer layer in the mixed halide $CH_3NH_3PbI_{3-x}Cl_x$ mesoporous perovskite solar cells, exhibited better characteristics than did with the reference appliance [153]. This improvement in characteristics using the mGO coating resulted from the arrangement of a homogeneous porosity observed in mGO film that possibly made way for the holes transport and thereby assisted the reducing charge recombination. Moreover, the hydrophobic behavior exhibited by mGO derivatives proved to be an additional shield to perovskite films that protected them from humidity, air, and therefore escalated the stability of manufactured PSCs. Table 1 summarizes the various parameters that are suitable for photovoltaic applications by making use of functionalized graphene nanocomposites. From the comparison of data, it can be observed that the $Fe_3O_4$–rGO composite has the superior photocurrent, followed by the

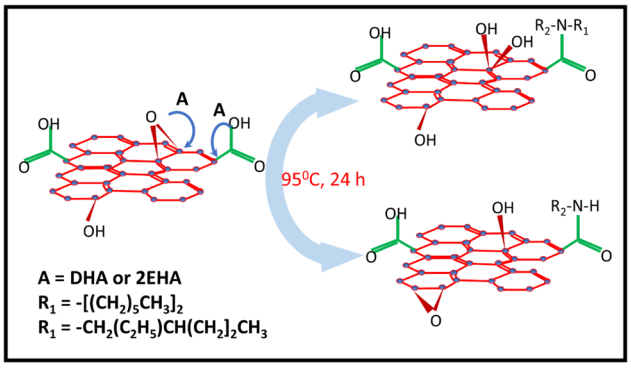


**Figure 18:** Schematic of the mechanism proposed for the binding of DHA and 2EHA onto the GO.

CoS/rGO, GO/$SnO_2$, and so on, and this suggests the importance of incorporating graphene with other metal oxide NPs to enhance the photocurrent in solar cells [154–156].

## 5.2 Electrochemical sensors

Taking into consideration of the fast-moving ability of graphene-based composites, Eshlaghi *et al.* [162] generated a sensor by integrating the GO surface [GO-imi-$(CH_2)_2$-$NH_2$] with the well-designed imidazole-$(CH_2)_2$-$NH_2$ group. This increases the surface area and conductivity of the composite that can be used for reasonable and sensitive recognition of Pb(II) in aqueous media (the whole

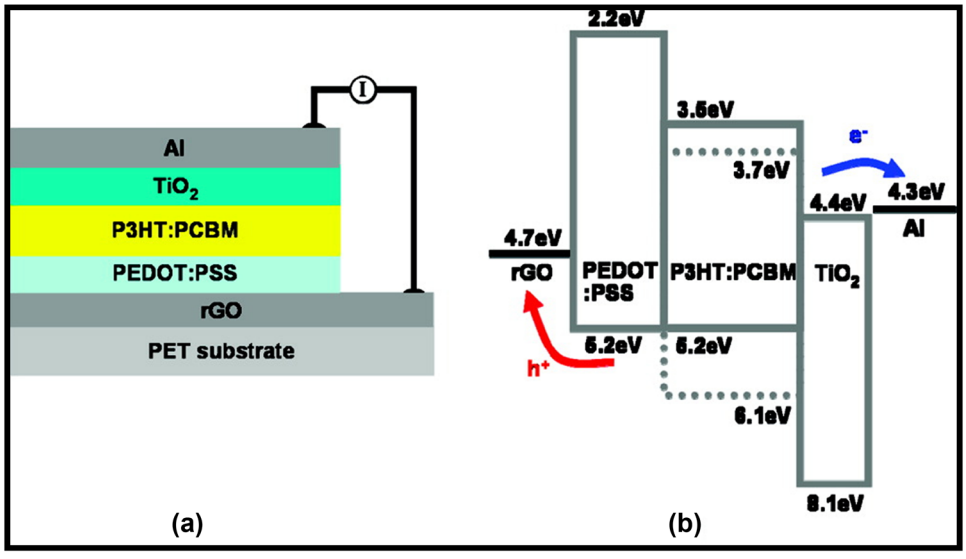


**Figure 17:** Schematic representation of (a) layer structure and (b) energy level for the OPV device, which is rGO/PEDOT:PSS/P3HT:PCBM/$TiO_2$/Al, with rGO as the transparent electrode [141]. PSS: poly (styrene sulfonate).

**Table 1:** Comparison of the various parameters of photovoltaic properties of functionalized graphene nanocomposites

| S. no. | Counter electrodes | Electrode | $J_{SC}$ (mA cm$^{-2}$) | $R_S$ (Ω cm$^2$) | $V_{OC}$ | FF | $\eta$ (%) | Ref. |
|---|---|---|---|---|---|---|---|---|
| 1 | rGO@PPy | Counter electrode | 7.49 | — | 0.70 | 0.42 | 2.2 | [157] |
| 2 | CoS/rGO | Counter electrode | 19.42 | 16.05 ± 0.02 | 0.76 | 0.63 | 9.3 | [154] |
| 3 | ZnO/rGO$_3$ | Photoanode | 3.02 | — | 0.64 | 0.60 | 1.5 | [158] |
| 4 | ZG + RB | Photoanode | 1.60 | — | 0.70 | 0.53 | 1.5 | [159] |
| 5 | $Fe_3O_4$–rGO | Counter electrode | 24.45 | — | 0.75 | 0.32 | 5.9 | [155] |
| 6 | $Fe_3O_4$–rGO | Counter electrode | 13.74 | 7.22 | 0.77 | 0.63 | 6.6 | [160] |
| 7 | $MoS_2$/graphene | Photoanode | 15.82 | — | 0.82 | 0.71 | 8.9 | [161] |
| 8 | GO/$SnO_2$ | Photoanode | 16.67 | — | 0.77 | 0.65 | 8.3 | [156] |

$J_{sc}$, short circuit current density; $R_S$, series resistance; $V_{oc}$, open circuit voltage; FF, fill factor; $\eta$, efficiency.

synthesis route is provided in Figure 19). The characterization of the composite cleared the favorable synthesis strategy of the GO-imi-$(CH_2)_2$-$NH_2$-CPE (conductive polymer electrode) grafting functional surface that can be used as a dependable Pb(II) sensor. Depending on the ideal conditions, the Pb(II) calibration diagram recorded linearly (−0.58 V) within the concentration range of 5.0–300.0 nM, and the high surface area and the solid Pb(II) adsorption capability with the good conductivity of the changed electrode suggested a reasonable Pb(II) detection limit of 0.30 nM. The electrode provided ease $-NH_2$ groups incorporating Pb(II) with good reusability up to five times and reproducibility of approximately 90%, which is satisfactory for electrochemical sensors.

Similarly, Wei *et al.* [163] used an rGO/$SnO_2$/Au composite for the electrochemical sensing of formaldehyde (HCHO), and its characterization revealed the formation of unique $SnO_2$ NSs decorated with Au NPs that are homogeneously attached to the rGO's surface. On testing, the gas-sensing analysis proved that the incorporation of $SnO_2$ NSs with Au NPs and rGO improved the gas-sensing for HCHO in terms of lower operating temperature, high sensor response, and good selectivity. The improved sensing properties could mainly be attributed to the synergism of the ohmic contact between rGO and $SnO_2$ NSs, high surface area, and strong gas-adsorption capacity of sheet-on-sheet heterostructure architectures and the catalytic effect of Au NPs. Finally, the work suggests that the rational design of 0D noble-metal NPs, 2D metal oxide NSs, and 2D rGO form ternary composites that provided an opportunity for the achievement of high-performance sensing materials.

## 5.3 Light-emitting and conducting diodes

For exploring the LED properties of GO-based composites, Wang *et al.* [164] with the use of spray coating technique fabricated a flexible TCF having the morphologies similar to reinforced concrete, *i.e.*, sandwiched the single-walled carbon nanotubes (SWCNT) between PEDOT:PSS and polydopamine-functionalized rGO (PDA-rGO), and the formed structure is expected to have enriched performance in the LED devices (the whole structure of final composite is schematically represented in Figure 20). Mussel-inspired PDA was popularized as a GO-reducing agent and modifier since the produced PDA–rGO was found to increase the interfacial bonding of sandwiching between the conductive coating layers and the substrate surface, which is a successful post-synthesis technique used for the hybrid film to attain improved conductivity. The electrode prepared by this method reported a low sheet resistance of 52.2 Ω sq$^{-1}$ along with improved optical transmittance of 88.7% at 550 nm. Moreover, these transparent films displayed long-standing stability with comparatively low roughness (about 2.41 nm), and its architecture maintained its flexibility throughout its bending course.

In a similar study, the composite film using PDA-rGO/SWCNT/PEDOT:PSS is formed to have applications as organic LEDs, where the device luminance is measured to be 2,032 cd cm$^{-2}$ at 15 V, the maximum current efficiency of 2.13 cd A$^{-1}$ at 14 V, thereby confirming for the presence of strong potentials that are especially applicable in flexible electroluminescent and photoelectric devices. Furthermore, Table 2 provides information about the various parameters and applicability of nanographene and its composites for the LED devices.

## 5.4 Optical and fiber-based biosensor probes

To test the efficacy of graphene-based composite biosensor probes, Xu *et al.* [170] promoted a label-free glucose biosensor that was effectively established and

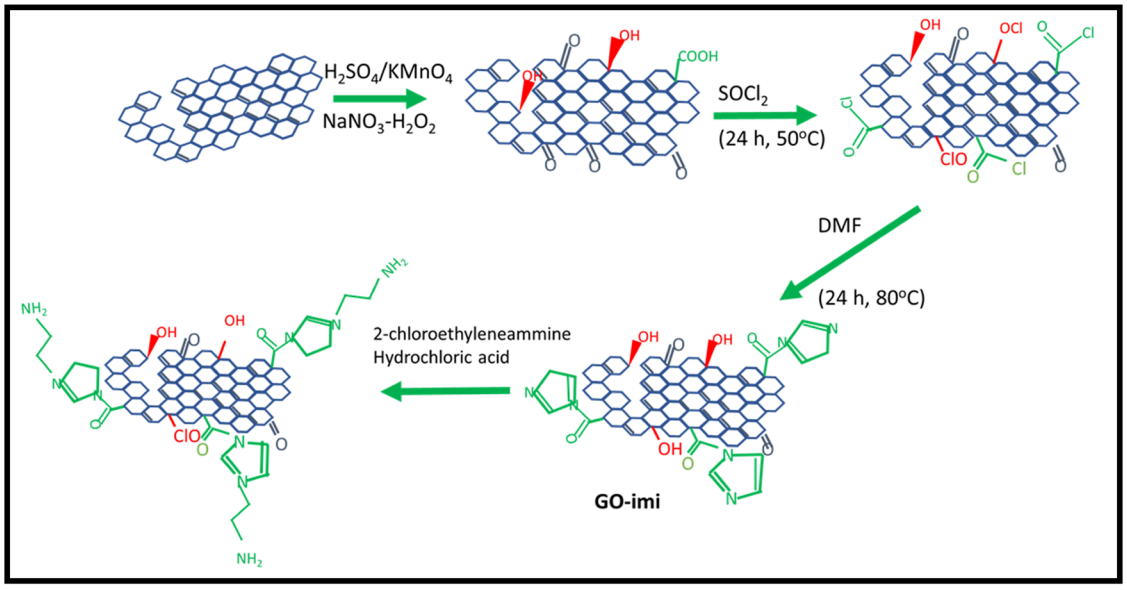


**Figure 19:** Schematic of synthesis process for the functionalized (GO-imi-$(CH_2)_2$-$NH_2$).

planted based on the long-period fiber grating (LPFG) functionalized GO-glucose oxidase (GOD) by means of chemical crosslinking (schematic of the biosensor construction is provided in Figure 21). Thus, the synthesized GO-coated LPFG surface is an ideal candidate for chemical and optical fiber sensing, because of the sensor's excellent operational environment, which can immobilize GOD by copious binding sites because of the constructive grouping of its remarkably large surface-to-volume ratio. It was found that gluconic acid and $H_2O_2$ were produced not only because of the major differences in the surrounding refractive index but also because of the reaction between GOD and glucose that leads to an obvious shift in the LPFG transmission spectrum. The optimum conditions of the sensory system include a 4 mg mL$^{-1}$ GOD concentration and a solution pH of 7, where the sensor has an excellent linear response even in the 0–1.2 mg mL$^{-1}$ low concentration range with a sensitivity of ~0.77 nm mg$^{-1}$ mL$^{-1}$. At the same time, the sensor showed a faster and shorter response time of 2.16 s. Furthermore, based on the selectivity and sensitivity of the developed detector, it can be confirmed that the developed biosensor can be used to detect practical samples in the pharmaceutical research and medical diagnosis fields.

In a different study [171], the GO–ZnS (GOZS) nanocomposite was successfully prepared by a solvothermal method (synthesis route for the composite formation is provided in Figure 22), where the characterization indicated for the even distribution of ZnS particles (20 nm diameter) onto the surface of GO that supported for an increase in the nonlinear absorption and optical limiting

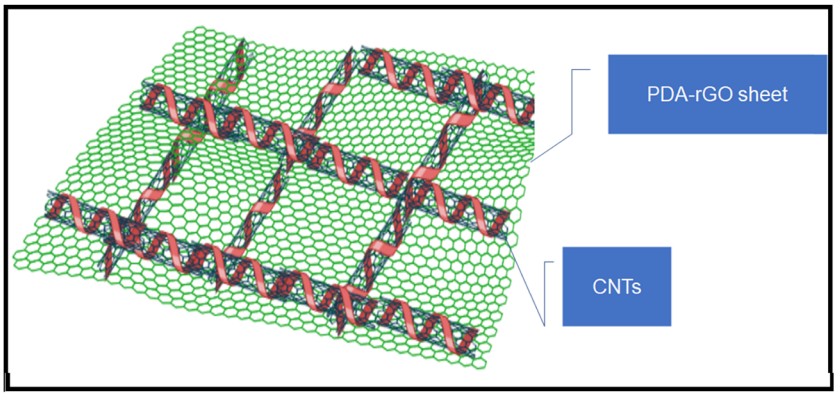


**Figure 20:** Schematic illustration of TCFs with ultra-adhesion, relatively low roughness, and excellent electrical conductivity.

**Table 2:** Comparison of various parameters (emission, quantum efficiency, *etc.*) of graphene and its functionalized nanocomposites

| S. no. | Material | Emission wavelength | Quantum efficiency (%) | Morphology | Particle size | Bandgap | Brightness (Cd $m^{-2}$) | Ref. |
|---|---|---|---|---|---|---|---|---|
| 1 | ZnO NP–rGO nanocomposite | Green | 0.22 | Hexagonal ZnO NPs | 30 nm | — | — | [165] |
| 2 | GQDs | White | 0.18 | Quasi-core–shell QDs | 10 nm | 250 meV | 798 | [166] |
| 3 | semi-rGO | Blue ($\lambda$ ~450 nm) to Red ($\lambda$ ~750 nm) | 1 | — | — | — | 6,000 | [167] |
| 4 | PLEDs with a 4.3 nm thick GO | Green (450 nm) | 6.7 | Graphene sheets | — | — | 39,000 | [168] |
| 5 | $MoS_2$–GO composites | Green | — | NSs | Up to 1 µm | — | 20,300 | [169] |

(OL) action of GOZS under ultrafast (1,030 nm, 340 fs) excitation. The calculated theoretical values of the nonlinear coefficients (at 20.8 GW $cm^{-2}$) of GO, ZnS, GOZS (4:5), GOZS (2:5), and GOZS (1:5) are 27.6, 25.4, 554.9, 193.3, and 117.1 cm $GW^{-1}$, respectively. Based on the Z-scan open-aperture investigation, the nonlinear activity elevated nearly 5- to 22-fold in GOZS as compared against pure GO and ZnS and is a result of the three-photon absorption of the sample. Moreover, the homogeneous delivery of ZnS NPs on the GO's surface increased their surface area as well as their dispersibility and consequently increased its light-absorption capacity. Furthermore, the conjugated structure of GO along with the 2D π-electron permits the composite to generate additional delocalized electrons. An improved absorption of free carriers and nonlinear activity was experienced, because the electron transport between GO layers and ZnS NPs inhibited the recombination of free carriers, as well as all these parameters, reinforcing the ability to organize it as an optical-limiting material.

## 5.5 Optical limiters

To test the efficacy of the charge transfer approach on optical properties, the three kinds of porphyrin–GO nanohybrids developed from the covalent functionalization method by Chen *et al.* [172] such as TPP-GO, TTP-GO, and TPP-GO-TTP are investigated to possess superior NLO absorption and OL characteristics. The effective charge transfer from the porphyrins to the nanohybrids of GO (schematic of its structural formation is provided in Figure 23) was confirmed by the Raman spectroscopy and other photophysical measurements. Also, within the three GO derivatives tested, the ternary hybrid of TPP-GO-TTP has exhibited superior NLO properties as compared to the other two and thereby emphasizing the importance of fine-tuning the photophysical and optical properties of nanohybrids through the introduction of porphyrins. Furthermore, the results generated from this study are potentially useful for the designing and development of various GO-mediated porphyrin derivatives that have applications in the NLO devices.

In a similar study [173], the nanocomposite of (3-aminopropyl)triethoxysilane (APTES) functionalized multilayer GO and its incorporation within the organosiloxane matrices formed by the sol–gel method (sequential synthesis is shown in Figure 24) are observed to maintain better NLO and optical-limiting properties than that of their GO precursor. Such an observed activity of GO–organosiloxane

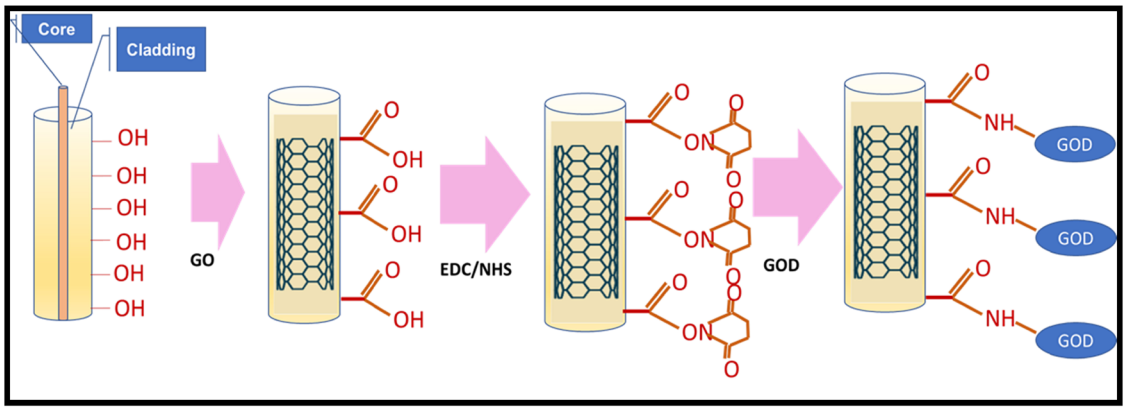


**Figure 21:** Schematic illustration of a fiber-optic biosensor based on GO-coated LPFG: FPLG surface with hydroxylation treatment, GO deposition, EDC/NHS-treated, and GOD-immobilized LPFG.

composite than that of pure multilayer GO can be linked to the occurrence of effective crosslinking among the two components that supported the generation of thermal microplasmas.

Graphene could be used as an EL material in nanoscale field-effect LED with tunable emission color [174]. Wang and co-workers have demonstrated a bright spectrally tunable EL ranging from blue (450 nm) to red (750 nm) at a reduced GO-based field-effect LED (GFLED) in Figure 25 [175]. They explained that the EL was caused by the recombination of Poole–Frenkel emission ionized electrons at the localized energy levels arising from semi-reduced GO and holes from the top of $\pi$ band (Figure 25).

## 5.6 Optical frequency converters

To test the influence of polarons and bipolar, and toward the optical frequency of nanocomposites having the grains separated by insulating regions, Dey *et al.* [176] studied the electrical transport properties of GO and n-PANI (polyaniline) composites (sequence of synthesis is shown in Figure 26). For the formation of GO–PANI composites, oxidative polymerization of aniline monomer with that of different weight percentages of GO was utilized. On testing the as-synthesized nanocomposite's electron transport properties against the variation of conductivity with those of temperature $T$ and $V$–I characteristics, the DC conductance

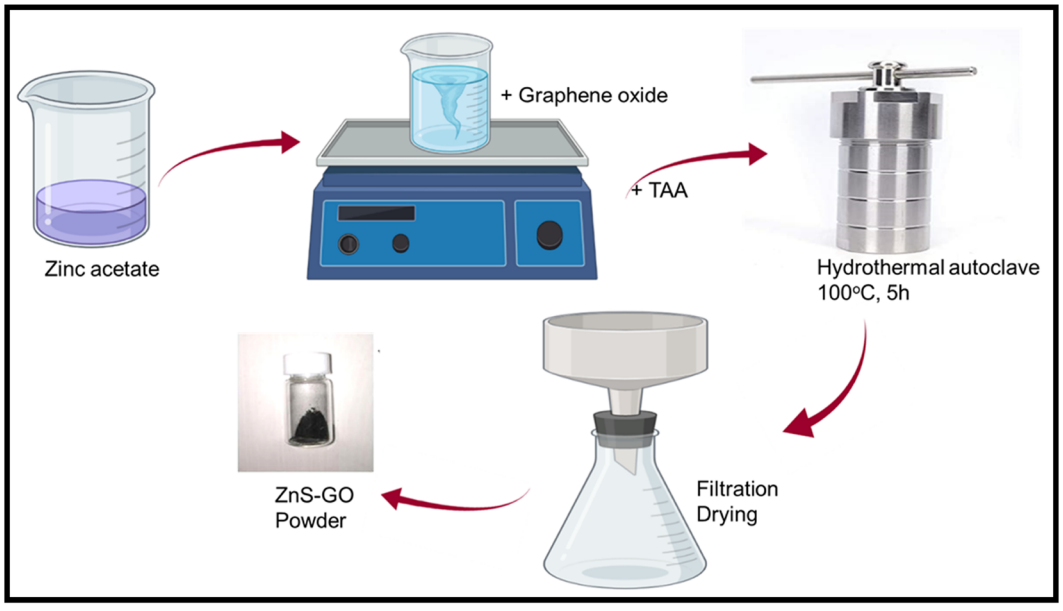


**Figure 22:** Schematic of the GOZS synthesis procedure starting from GO with the addition of zinc compound, followed by the heating and filtration to finally produce the composite in black colored powder.

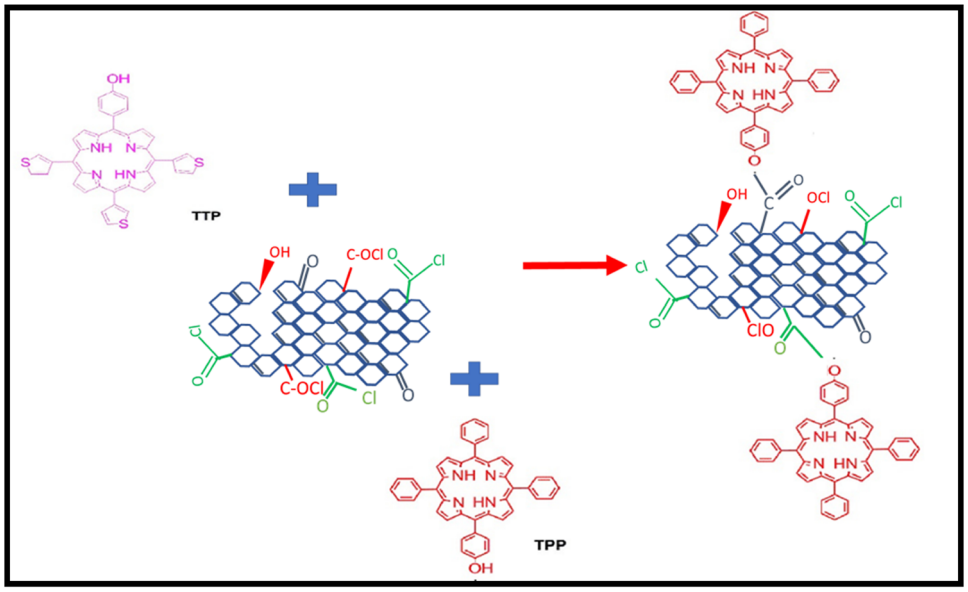


**Figure 23:** Synthetic route for the formation of TPP-GO-TTP nanohybrids.

at Σ indicated a behavioral change from the insulator-type to low-temperature-dependent behavior (at temperature $T_D$). The $V$–$I$ characteristics, in general, are nonlinear, and such nonlinear property seems to be increased with that of decreased temperature. For the studies where the temperatures are greater than $T_D$ ($T \geq T_D$), the high voltage values were observed at higher currents, close to the Zener diodes. However, for the studies of lower temperatures ($T \leq T_D$), the maximum voltages observed as similar to that of thyristors and so can be utilized for the manufacturing of devices that can exhibit the controlled electrical and insulating properties. From the cumulative analysis, two different phases were noticed for the nanocomposites over the measured temperature range, *i.e.*, an insulating-type of behavior (from room temperature to $T_D$) and a low-temperature-dependent behavior (below $T_D$ down to 10 K). Also, it was observed that $T_D$ is dependent on GO's weight percentages, and the formed nanocomposite's $V$–$I$ characteristics have exhibited non-ohmic electrical conduction and is characterized by the onset voltage ($V_0$), which scales with the ohmic conductance ($\Sigma_0$) and nonlinearity exponent ($x_T$). The weight percentages of GO are investigated to have negative $x_T$ values and further, all the observed results were explained based on the nanocomposite's grain structure.

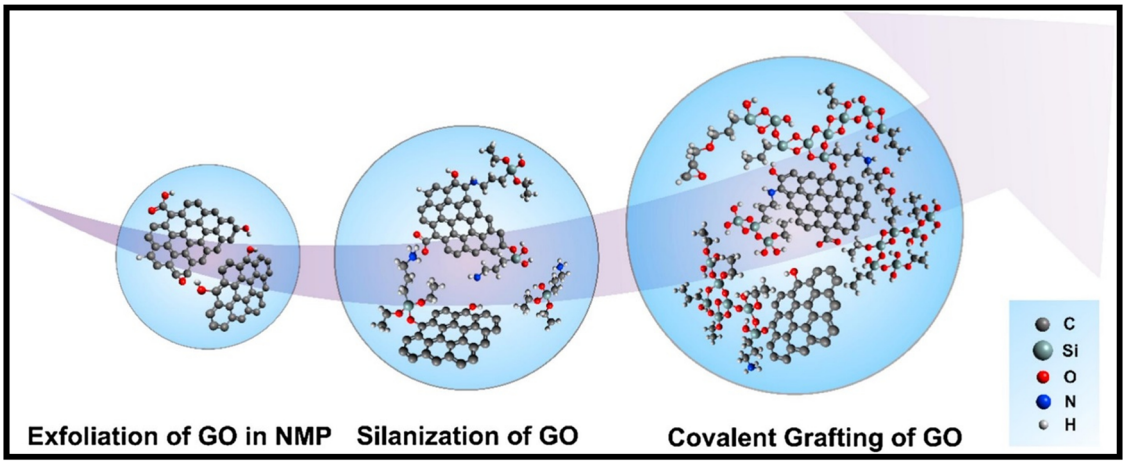


**Figure 24:** Schematic diagrams for the preparation of GO functionalized with APTES incorporated in an organosiloxane matrix (f-GO/sol) [173].

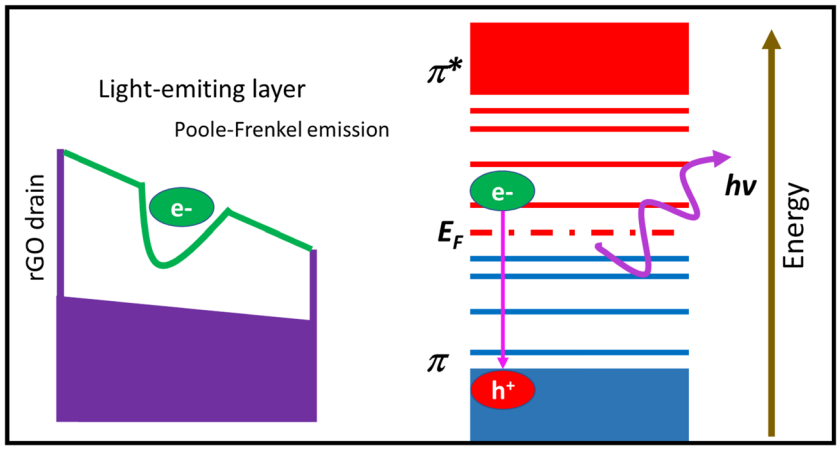


**Figure 25:** Scheme for the charge injection process of GFLED.

## 5.7 Transparent conductors

In another study conducted by Compton and his co-workers [177], several conductive "alkylated" graphene sheets were synthesized by a one-pot process by modifying the synthesized GO layers with hexylamine (HA) followed by a hydrazine reduction reaction (synthesis for the bonding of alkylated aniline with that of GO is represented in Figure 27). The "alkylation process" with HA not only preserved the stacked-layer arrangement throughout the reduction course but also maintained its well-organized morphology as well as ensuring its

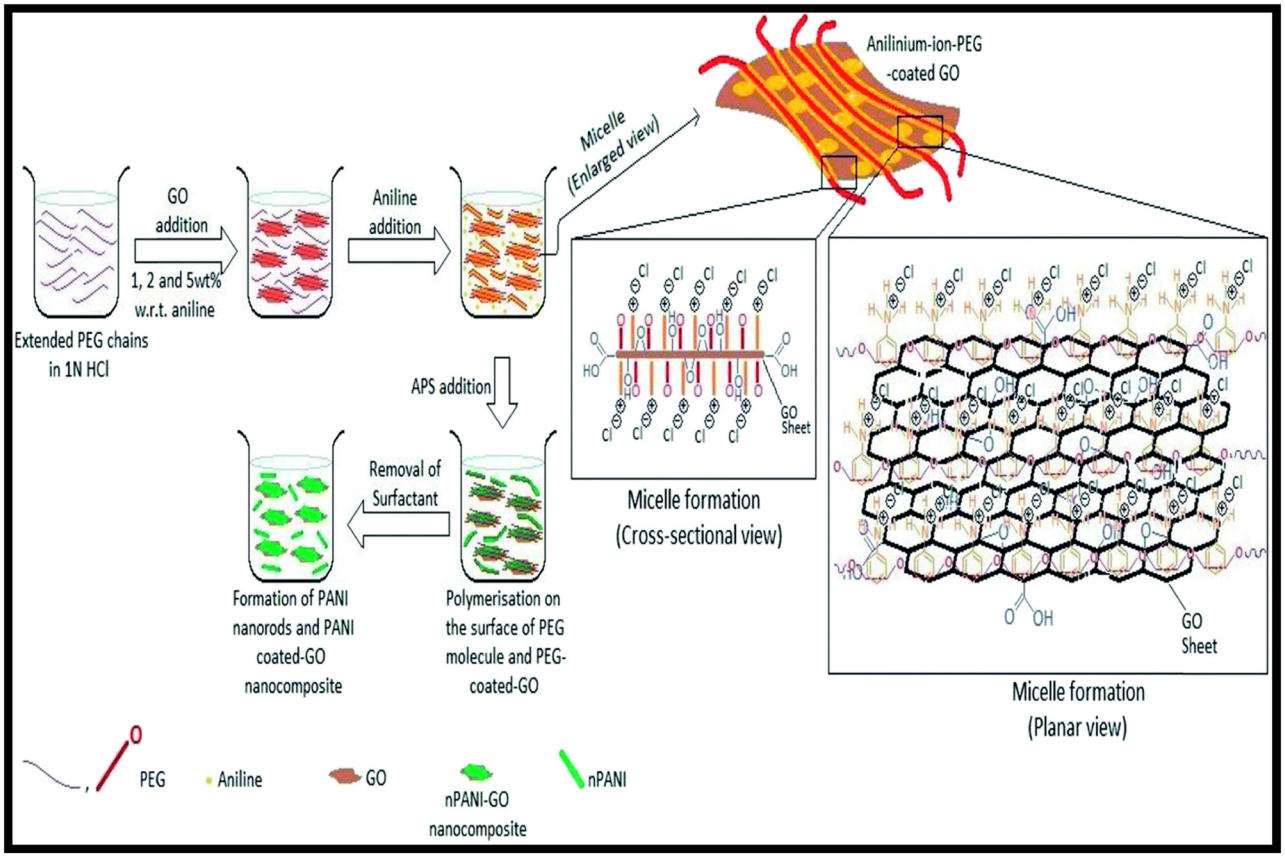


**Figure 26:** Various steps are involved in the preparation of n-PANI–GO composites along with the representation of both cross-sectional and planar views of the intermediate structures [176].

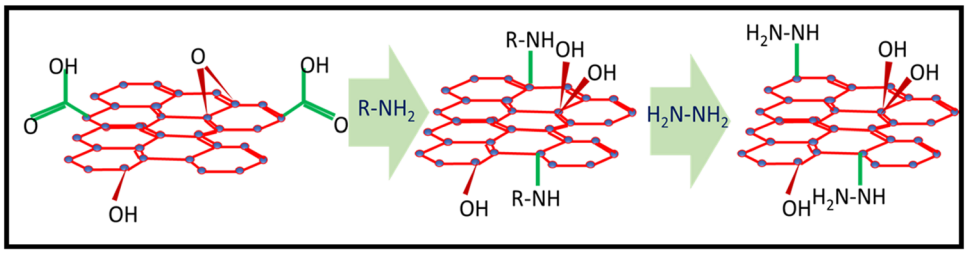


**Figure 27:** Scheme of amine bonding in HA–GO and HA–graphene papers.

consistent conductivity and excellent mechanical properties. The altered amine–alkylate-stacked GO layers produced a stable organization, because of the precise hydrazine-reduction environment. Thus, the resulting "alkylated" graphene sheet had a well-organized morphology along with uniform conductivity, as associated with graphene sheets synthesized without the influence of amines. Therefore, these chemical modification techniques can be used as a smart approach for designing favorable blends and structures with desired characteristics in co-operated graphene sheets. Nevertheless, these "alkylated" graphene sheets can be used as novel materials for various applications. As an example, it is preferred to have the biocompatible material consisting of large pores or integral spaces, which can support the encapsulation of enzymes and the growth of cells. Also, integral functionalization can transform graphene paper into a high-capacity, well-ordered ion-storage medium for supercapacitors and LiBs. Table 3 shows the transparent and electron-conducting efficiency of various kinds of functionalized graphene.

## 5.8 Terahertz devices

The terahertz electromagnetic interference (EMI) materials were constructed by Lin *et al.* [183] in an ion-diffusion gelation method with the cross-linking of GO and MXene sheets (2D transition metal carbides and/or nitrides) multivalent metal ions (synthesis scheme and physicochemical characterizations are represented in Figure 28). Thus, formed sheets having porous structures have effectively reduced radiation pollution by serving as a shield. The testing has shown that the MXene foam material having the cross-linked porous structure was promising for the EMI shielding and simultaneously suitable because of its lightweight, high stability, foldable nature in wet environments, and excellent terahertz shielding ability of 51 dB even at a narrow thickness of 85 µm. This study results for the first time have provided an insight into the usage of 3D macroscopic MXenes as high-performance terahertz shielding materials.

In a similar study to test the efficacy of organic materials in LiBs, Li *et al.* [184] identified that the electrode materials made from graphene and CNTs ($C_{60}(OH)_{12}$) have possessed a high specific capacity that can promise for an increase of energy efficiency. For the studies, the CNTs/GO anode materials were formed by the uniform growth of CNTs onto the surfaces of GO NSs (bonding of CNTs carboxyl and epoxy groups). The synthesis route along with the morphological analysis are presented in Figure 29. On testing, the CNTs/GO anode material is found to have superior battery performance by having the reversible capacity of 1,596 mA h $g^{-1}$ at 0.2 A $g^{-1}$, which is higher than that of the individual capacities of CNTs and GO, thereby confirming the potential applicability of CNTs/GO nanocomposite for the high-performance LiBs and other conducting applications.

**Table 3:** Overview of the synthesis method and transparent conducting behavior of graphene-based nanocomposites

| S. No. | Material | Preparation method | Transmission rate (%) | Sheet resistance (Ω $sq^{-1}$) | Ref. |
|---|---|---|---|---|---|
| 1 | CVD graphene on Ag NW | — | 88 | 22 | [178] |
| 2 | Graphene/PEDOT:PSS, hybrid ink | Spray coating | 80 | 600 | [179] |
| 3 | CVD graphene on ITO film | — | 88.25 | 76.46 | [180] |
| 4 | Graphene/CuNW-core/shell structure | — | 79 | 36 | [181] |
| 5 | Graphene/ITO NPs | CVD | 85 | 522 | [182] |

## 5.9 Photodetectors

Li *et al.* [185] employed a one-pot hydrothermal method for the synthesis of rGO that was additionally used to prepare a nanocomposite consisting of hemin *via* π interactions. Following that, the hemin–rGO nanocomposite was incorporated into the Nafion film and then placed on a glassy carbon electrode (GCE). Thus, modified GCE on testing showed exceptional catalytic properties toward $H_2O_2$, and such activity can be linked to the presence of hemin's redox-active center [Fe(III/II)] and foam's cross-linked macroporous structure. Furthermore, on testing, the electrode has exhibited a typical working voltage of −0.41 mV (*vs* SCE), sensitivity (detection limit of $H_2O_2$) of 2.8 nM, and for the concentration in the range of 5 nM to 5 mM, a sensitivity of 50.5 μA $\mu M^{-1}$ $cm^{-2}$ was observed. From the analysis, the authors have confirmed that the modified GCE electrode has a fast response and is highly sensitive and thus so can be used for the qualitative and quantitative analysis of $H_2O_2$ samples.

Similarly, transition metal composites were formed using the sonochemical technique, *i.e.*, Palanisamy *et al.* [186] prepared CuS nanoplates partially decorated with an rGO (PrGO) nanocomposite (sonication frequency of 37 kHz, power of 150 W). The synthesis scheme and reaction conditions along with the microstructure of the product are shown in Figure 30. On testing the electroanalytical performance of dopamine neurotransmitters, the PrGO–CuS nanocomposite was investigated to have far better activity than that of the corresponding components of GO, CuS, and GO–CuS composites individually. With the use of the PrGO–CuS electrode sensor, dopamine was identified even to a lower detection limit of 0.022 μM with a more extensive linear response range of 0.1–155 μM, and a quantitation limit of 2.6 nM. Thus, from the cumulative analysis of results, the fabricated electrode of PrGO–CuS nanocomposite has superior selectivity with acceptable storage and cyclic stability, and therefore, can be applied for the successful detection of dopamine in any kind of samples. The summary of functionalized graphene nanocomposites as photodetectors is provided in Table 4.

# 6 Conclusion and future directions

In conclusion, in this review, we stress the importance of forming composites containing GO layers to obtain results better than those of the basic ones. Since the

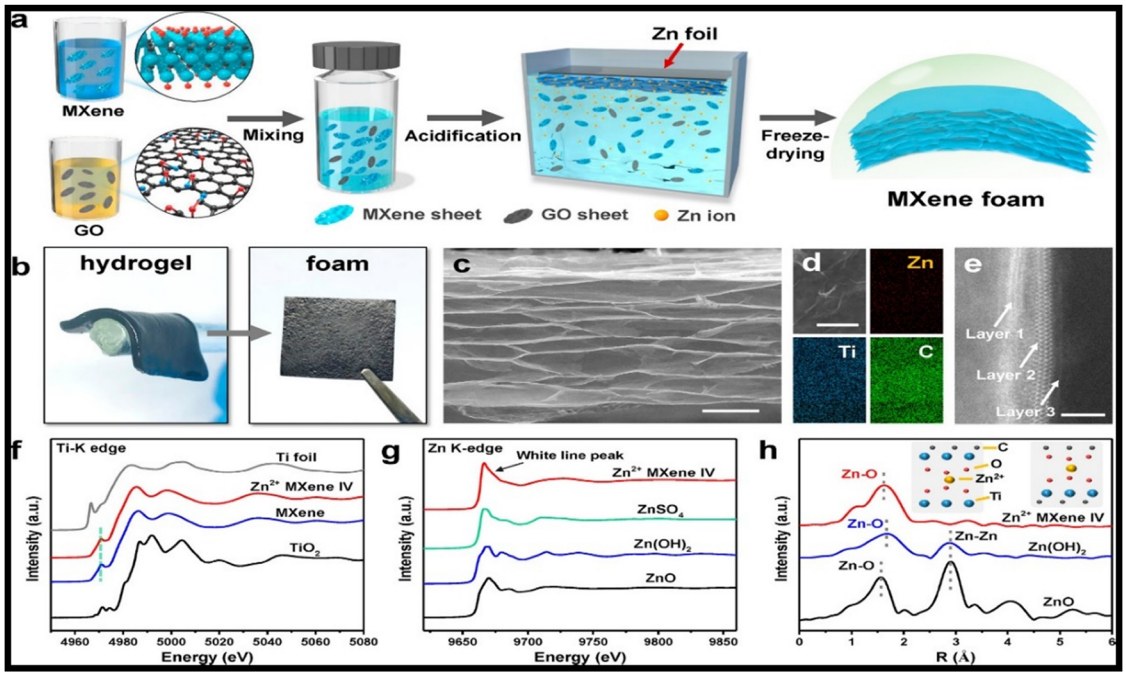


**Figure 28:** (a) Schematic representation of ion-diffusion-induced gelation process, (b) free-standing and flexible $Zn^{2+}$ MXene IV hydrogel and foam, (c) cross-sectional scanning electron microscopy, (d) energy-dispersive X-ray spectroscopic elemental mapping, (e) high-angle annular dark-field scanning transmission electron microscopy images of the $Zn^{2+}$ MXene IV foam, (f) Ti K-edge X-ray absorption near-edge structure, (g) Zn K-edge, and (h) Fourier transform extended X-ray absorption fine-structure spectra of the $Zn^{2+}$ MXene IV foam and references. Scale bars: (c) 50 μm, (d) 5 μm, (e) 2 nm [183].

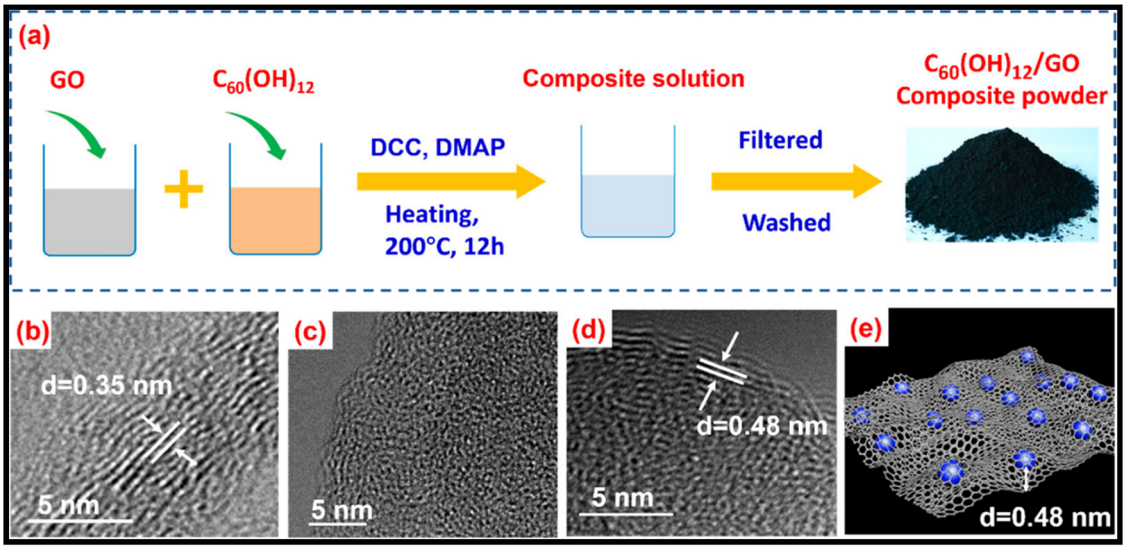


**Figure 29:** (a) Synthetic route for the active material of the LIB anode: the $C_{60}(OH)_{12}$/GO composite. High-resolution TEM images of (b) GO, (c) $C_{60}(OH)_{12}$ NPs, and (d) the $C_{60}(OH)_{12}$/GO composite; the *d*-spacing is found by estimating the distance between the two white lines. (e) Schematic diagram showing the $C_{60}(OH)_{12}$/GO composite with $C_{60}$ molecules embedded between GO layers [184].

graphene or its nanocomposites formed with other metal oxides, polymers, or other molecules are expected to benefit the ever-demanding sectors such as energy, electronics, catalysis, remediation, biosensing, and sustainability, the material can have a significant role from the commercial–industrial aspects too. For all these applications, the most influential factors are the sensitivity points, size, shape, surface area and charges, porosity, and hydrophobicity to affect the mechanical resistance, optical properties, adsorption capacity, thermal conductivity, and electrical mobility. To maintain the abovementioned characteristics of the graphene-based nanocomposites, both materials should covalently bound to each other, and in some cases, the van der Waals forces may play a critical role. Although a significant achievement has been generated in other application areas with graphene, there is still a

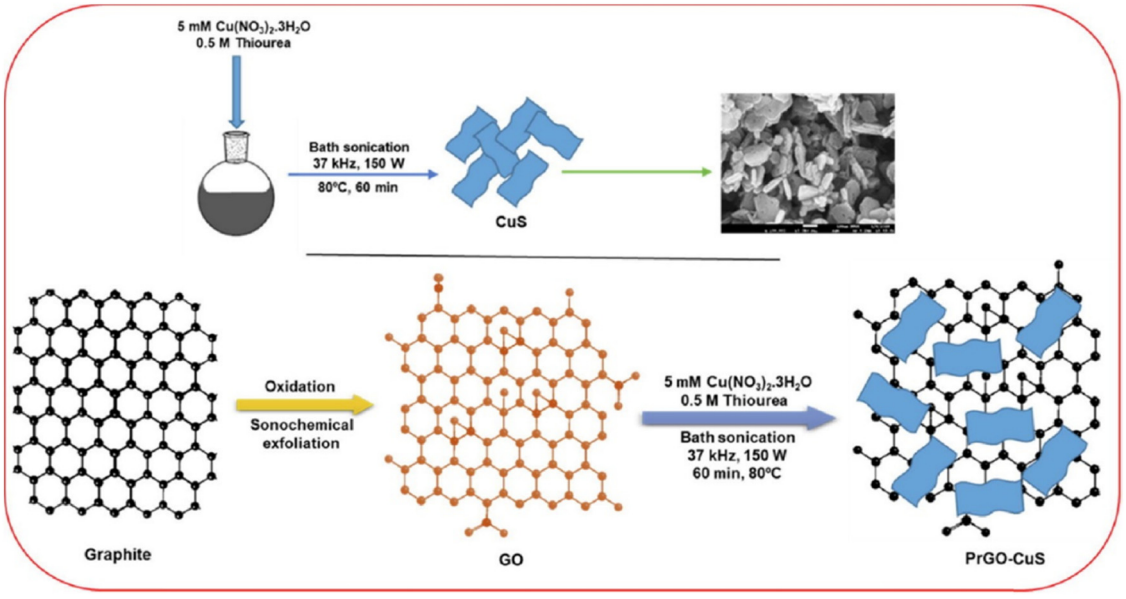


**Figure 30:** Schematic illustration of the sonochemical preparation of CuS and PrGO–CuS nanocomposite (189).

**Table 4:** Overview of the various parameters supporting the photo-detecting behavior of functionalized graphene nanocomposites

| S. No. | Material | Responsivity | Specific detectivity | Photo response wavelength (nm) | Photoconductive gain | Ref. |
|---|---|---|---|---|---|---|
| 1 | GMG | $2 \times 10^3$ mA W$^{-1}$ | $10^{13}$ Jones | 450–680 | 54 | [187] |
| 2 | GQDs decorated n-ZnO/n-GaN | 34 mA W$^{-1}$ | up to ~$10^{12}$ Jones | 365 | — | [188] |
| 3 | P3HT/graphene composite | 0.25 A W$^{-1}$ | $1.8 \times 108$ Jones | 380–750 | — | [189] |
| 4 | Large-area graphene/$MoS_2$ | 45.5 A W$^{-1}$ | — | 642 | $4 \times 10^5$ | [190] |
| 5 | GO-modified $TiO_2$ | 826.8 A W$^{-1}$ | $2.82 \times 10^{13}$ cm Hz$^{1/2}$ W$^{-1}$ | 280 | — | [191] |

limited role in especially the biomedical sector. Since graphene and its compounds are mostly hydrophobic, to explore the role of graphene and its composites in the biomedical sector, research should focus on increasing the hydrophilic capacity while simultaneously maintaining the hybrid properties from all of the individual components.

Second, the ecological and biological toxicity of graphene-based nanocomposites has yet to be understood, since it has not received much attention. However, in some applications, like drug delivery and bioimaging, graphene has shown great potential, its cell toxicity and ecological organism still need to be studied. Graphene and its nanocomposites are biocompatible in some cases but not all. Therefore, a rational understanding is required for the biocompatibility of graphene. Third, to explore these composites in the bioanalytical sector for the qualitative and quantitative analysis of a range of analytes, including the antibodies, nucleic acids, proteins, and bacteria, the need for the development of graphene-based electrochemical sensors with sensitivity and specificity should not be ignored. One approach to developing affordable, specific, sensitive, and user-friendly devices is by making use of the layer-by-layer assembling technology for the development of lab-on-a-chip devices involving graphene as a sensory probe, where the formed probe can help in analyzing a range of samples from the pharmaceutical, water and environmental, food and agriculture, and forensic domains.

We are expecting more development in the above-mentioned directions using graphene and its nanocomposites in future decades, since graphene is the most important discovery in recent decades in the field of condensed physics and material science. Being the thinnest material in the universe, graphene can help in increasing the understanding of workers in fundamental and advanced research. We believe that graphene and its derivatives along with other 2D crystals can greatly affect human life by the development of brand-new technologies in the future.

**Funding information:** This work was supported by the University of Malaya Research Grant (RU001-2019, RU001-2020) and the International Postdoctoral Exchange Fellowship Programme of China.

**Author contributions:** All authors have accepted responsibility for the entire content of this manuscript and approved its submission.

**Conflict of interest:** The authors state no conflict of interest.

**Data availability statement:** All data generated or analysed during this study are included in this published article.

## References


[1] Nag A, Mitra A, Mukhopadhyay SC. Graphene and its sensor-based applications: a review. Sens Actuators A: Phys. 2018;270:177–94.

[2] Lingamdinne LP, Koduru JR, Karri RR. A comprehensive review of applications of magnetic graphene oxide-based nanocomposites for sustainable water purification. J Environ Manag. 2019;231:622–34.

[3] Kuilla T, Bhadra S, Yao D, Kim NH, Bose S, Lee JH. Recent advances in graphene-based polymer composites. Prog Polym Sci. 2010;35(11):1350–75.

[4] Shahid MM, Ismail AH, AL-Mokaram AMAA, Vikneswaran R, Ahmad S, Hamza A, et al. A single-step synthesis of nitrogen-doped graphene sheets decorated with cobalt hydroxide nanoflakes for the determination of dopamine. Prog Nat Sci: Mater Int. 2017;27(5):582–7.

[5] Shahid MM, Pandikumar A, Golsheikh AM, Huang NM, Lim HN. Enhanced electrocatalytic performance of cobalt oxide nanocubes incorporating reduced graphene oxide as a modified platinum electrode for methanol oxidation. RSC Adv. 2014;4(107):62793–801.

[6] Shahid MM, Rameshkumar P, Basirun WJ, Juan JC, Huang NM. Cobalt oxide nanocubes interleaved reduced graphene oxide as an efficient electrocatalyst for oxygen reduction reaction in alkaline medium. Electrochim Acta. 2017;237:61–8.

[7] Marlinda AR, Sagadevan S, Yusoff N, Pandikumar A, Huang NM, Akbarzadeh O, et al. Gold nanorods-coated reduced graphene oxide as a modified electrode for the electrochemical sensory detection of NADH. J Alloy Compd. 2020;847:156552.

[8] Shahid MM, Rameshkumar P, Huang NM. A glassy carbon electrode modified with graphene oxide and silver nanoparticles for amperometric determination of hydrogen peroxide. Microchim Acta. 2016;183(2):911–6.

[9] Sagadevan S, Chowdhury ZZ, Rafie Bin Johan M, Khan AA, Aziz FA, Rafique RF, et al. A facile hydrothermal approach for catalytic and optical behavior of tin oxide-graphene ($SnO_2$/G) nanocomposite. PLOS One. 2018;13(10):e0202694.

[10] Sagadevan S, Pal K, Chowdhury ZZ. Controllable synthesis of graphene/ZnO-nanocomposite for novel switching. J Alloy Compd. 2017;728:645–54.

[11] Sagadevan S, Pal K, Chowdhury ZZ. Scalable synthesis of CdS-graphene nanocomposite spectroscopic characterizations. J Mater Sci: Mater Electron. 2017;28:17193–201.

[12] Rahman MA, Tong GB, Kamaruddin NH, Abd Wahab F, Hamizi NA, Chowdhury ZZ, et al. Effect of graphene infusion on morphology and performance of natural rubber latex/graphene composites. J Mater Sci: Mater Electron. 2019;30:12888–94.

[13] Zhu Y, Murali S, Cai W, Li X, Suk JW, Potts JR, et al. Graphene and graphene oxide: synthesis, properties, and applications. Adv Mater. 2010;22(35):3906–24.

[14] Kumar R, Singh R, Hui D, Feo L, Fraternali F. Graphene as biomedical sensing element: state of art review and potential engineering applications. Compos Part B: Eng. 2018;134:193–206.

[15] Oh W-C, Fatema KN, Liu Y, Jung CH, Sagadevan S, Biswas MdRUdD. Polypyrrole-bonded quaternary semiconductor $LiCuMo_2O_{11}$ – Graphene nanocomposite for a narrow band gap energy effect and its gas-sensing performance. ACS Omega. 2020;5:17337–46.

[16] Sagadevan S, Pal K, Koteeswari P, Subashini A. Synthesis and characterization of $TiO_2$/graphene oxide Nanocomposite. J Mater Sci: Mater Electron. 2017;28:7892–8.

[17] Sagadevan S, Das I, Pal K, Murugasen P, Singh P. Optical and electrical smart response of chemically stabilized graphene oxide. J Mater Sci: Mater Electron. 2017;28:5235–43.

[18] Marlinda AR, Yusoff N, Sagadevan S, Johan MR. Recent developments in reduced graphene oxide nanocomposites for photoelectrochemical water-splitting applications. Int J Hydrog Energy. 2020;45:11976–94.

[19] Sagadevan S, Chowdhury ZZ, Hoque MdE, Podder J. Chemically stabilized reduced graphene oxide/zirconia nanocomposite: synthesis and characterization. Mater Res Express. 2017;4:115031.

[20] Sagadevan S, Chowdhury ZZ, Rafie Bin Johan Md, Rafique RF, Aziz FA. One pot synthesis of hybrid ZNS-graphene nanocomposite with enhanced photocatalytic activities using hydrothermal approach. J Mater Science: Mater Electron. 2018;29:9099–107.

[21] Kamaruddin NH, Marlinda AR, Said M, Wahab FA, Tong GB, Hamizi NA, et al. Synergistic effects of rubber band infused graphene nanocomposite on morphology, spectral, and dynamic mechanical properties. Polym Compos. 2020;41:1475–80.

[22] Sagadevan S, Rafie Johan Md, Anita Lett J. Fabrication of reduced graphene oxide/$CeO_2$ nanocomposite for enhanced electrochemical performance. Appl Phys A. 2019;125:315.

[23] Sagadevan S, Chowdhury ZZ, Rafie Bin Johan M, Aziz FA, Roselin LS, Hsu H-L, et al. Synthesis, characterization and electrochemical properties of cadmium sulfide - Reduced graphene oxide nanocomposites. Results Phys. 2019;12:878–85.

[24] Novoselov KS, Fal'ko VI, Colombo L, Gellert PR, Schwab MG, Kim K. A roadmap for graphene. Nature. 2012;490(7419):192–200.

[25] Papageorgiou DG, Kinloch IA, Young RJ. Mechanical properties of graphene and graphene-based nanocomposites. Prog Mater Sci. 2017;90:75–127.

[26] Novoselov KS, Geim AK, Morozov SV, Jiang D, Zhang Y, Dubonos SV, et al. Electric field effect in atomically thin carbon films. Science. 2004;306(5696):666–9.

[27] Sagadevan S, Chowdhury ZZ, Johan MRB, Rafique RF. A facile one-step hydrothermal synthesis of $HfO_2$/graphene nanocomposite and its' physio-chemical properties. Mater Res Express. 2018;5:035014.

[28] Sagadevan S, Chowdhury ZZ, Rafie Bin Johan Md, Aziz FA, Salleh EM, Hawa A, et al. A one-step facile route synthesis of copper oxide/reduced graphene oxide nanocomposite for supercapacitor applications. J Exp Nanosci. 2018;13(1):302–13.

[29] Xue Y, Liu J, Chen H, Wang R, Li D, Qu J, et al. Nitrogen-doped graphene foams as metal-free counter electrodes in high-

performance dye-sensitized solar cells. Angew Chem Int Ed. 2012;51(48):12124–7.
[30] Xu Y, Sheng K, Li C, Shi G. Self-assembled graphene hydrogel *via* a one-step hydrothermal process. Acs Nano. 2010;4(7):4324–30.
[31] Duplock EJ, Scheffler M, Lindan PJ. Hallmark of perfect graphene. Phys Rev Lett. 2004;92(22):225502.
[32] Sheehy DE, Schmalian J. Optical Transpar graphene determined fine-structure constant. Phys Rev B. 2009;80(19):193411.
[33] Novoselov KS, Geim AK, Morozov SV, Jiang D, Zhang Y, Dubonos SV, et al. Electric field effect in atomically thin carbon films. Science. 22 Oct 2004;306(5696):666–9.
[34] Geim AK. Graphene: status and prospects. Science. 2009;324(5934):1530–4.
[35] Ikhsan NI, Rameshkumar P, Pandikumar A, Shahid MM, Huang NM, Kumar SV, et al. Facile synthesis of graphene oxide–silver nanocomposite and its modified electrode for enhanced electrochemical detection of nitrite ions. Talanta. 2015;144:908–14.
[36] Shahabuddin S, Sarih NM, Ismail FH, Shahid MM, Huang NM. Synthesis of chitosan grafted-polyaniline/$Co_3O_4$ nanocube nanocomposites and their photocatalytic activity toward methylene blue dye degradation. RSC Adv. 2015;5(102):83857–67.
[37] Sagadevan S, Marlinda AR, Johan MR, Umar A, Fouad H, Alothman OY, et al. Reduced graphene/nanostructured cobalt oxide nanocomposite for enhanced electrochemical performance of supercapacitor applications. J Colloid Interface Sci. 2019;558:68–77.
[38] Heath J, Zhang Q, O'Brien S, Curl R, Kroto H, Smalley R. The formation of long carbon chain molecules during laser vaporization of graphite. J Am Chem Soc. 1987;109(2):359–63.
[39] Iijima S. Helical microtubules of graphitic carbon. Nature. 1991;354(6348):56.
[40] Kauffman DR, Star A. Graphene versus carbon nanotubes for chemical sensor and fuel cell applications. Analyst. 2010;135(11):2790–7.
[41] Fasolino A, Los J, Katsnelson MI. Intrinsic ripples in graphene. Nat Mater. 2007;6(11):858.
[42] Antonietti M, Müllen K. Carbon: the sixth element. Adv Mater. 2010;22(7):787.
[43] Liang H-W, Zhuang X, Brüller S, Feng X, Müllen K. Hierarchically porous carbons with optimized nitrogen doping as highly active electrocatalysts for oxygen reduction. Nat Commun. 2014;5:4973.
[44] Park S, Ruoff RS. Chemical methods for the production of graphenes. Nat Nanotechnol. 2009;4(4):217.
[45] Lu X, Yu M, Huang H, Ruoff RS. Tailoring graphite with the goal of achieving single sheets. Nanotechnology. 1999;10(3):269.
[46] Pan D, Wang S, Zhao B, Wu M, Zhang H, Wang Y, et al. Li storage properties of disordered graphene nanosheets. Chem Mater. 2009;21(14):3136–42.
[47] Guo H-L, Wang X-F, Qian Q-Y, Wang F-B, Xia X-H. A green approach to the synthesis of graphene nanosheets. ACS Nano. 2009;3(9):2653–9.
[48] Kim KS, Zhao Y, Jang H, Lee SY, Kim JM, Kim KS, et al. Large-scale pattern growth of graphene films for stretchable transparent electrodes. Nature. 2009;457(7230):706.
[49] Sutter PW, Flege J-I, Sutter EA. Epitaxial graphene on ruthenium. Nat Mater. 2008;7(5):406.
[50] Rao CNR, Sood AK, Subrahmanyam KS, Govindaraj A. Graphene: the new two-dimensional nanomaterial. Angew Chem Int Ed. 2009;48(42):7752–77.
[51] Choucair M, Thordarson P, Stride JA. Gram-scale production of graphene based on solvothermal synthesis and sonication. Nat Nanotechnol. 2009;4(1):30.
[52] Berger C, Song Z, Li X, Wu X, Brown N, Naud C, et al. Electronic confinement and coherence in patterned epitaxial graphene. Science. 2006;312(5777):1191–6.
[53] Yang J, Deng S, Lei J, Ju H, Gunasekaran S. Electrochemical synthesis of reduced graphene sheet–AuPd alloy nanoparticle composites for enzymatic biosensing. Biosens Bioelectron. 2011;29(1):159–66.
[54] Liu N, Luo F, Wu H, Liu Y, Zhang C, Chen J. One-step ionic-liquid-assisted electrochemical synthesis of ionic-liquid-functionalized graphene sheets directly from graphite. Adv Funct Mater. 2008;18(10):1518–25.
[55] Kim H, Abdala AA, Macosko CW. Graphene/polymer nanocomposites. Macromolecules. 2010;43(16):6515–30.
[56] Dresselhaus G, Riichiro S. Physical properties of carbon nanotubes. Singapore: Imperial College Press; 1998.
[57] Neto AC, Guinea F, Peres NM. Drawing conclusions from graphene. Phys World. 2006;19(11):33.
[58] Katsnelson M, Novoselov K, Geim A. Chiral tunnelling and the Klein paradox in graphene. Nat Phys. 2006;2(9):620–5.
[59] Katsnelson M, Novoselov K. Graphene: new bridge between condensed matter physics and quantum electrodynamics. Solid State Commun. 2007;143(1–2):3–13.
[60] Zhang Y, Tan Y-W, Stormer HL, Kim P. Experimental observation of the quantum Hall effect and Berry's phase in graphene. Nature. 2005;438(7065):201.
[61] Geim AK, Novoselov KS. The rise of graphene. Nanoscience and technology: a collection of reviews from nature journals. London, United Kingdom: World Scientific; 2010. p. 11–9
[62] Du X, Skachko I, Barker A, Andrei EY. Approaching ballistic transport in suspended graphene. Nat Nanotechnol. 2008;3(8):491.
[63] Nair RR, Blake P, Grigorenko AN, Novoselov KS, Booth TJ, Stauber T, et al. Fine structure constant defines visual transparency of graphene. Science. 2008;320(5881):1308.
[64] Iorsh IV, Mukhin IS, Shadrivov IV, Belov PA, Kivshar YS. Hyperbolic metamaterials based on multilayer graphene structures. Phys Rev B. 2013;87(7):075416.
[65] Chang Y-C, Liu C-H, Liu C-H, Zhang S, Marder SR, Narimanov EE, et al. Realization of mid-infrared graphene hyperbolic metamaterials. Nat Commun. 2016;7(1):1–7.
[66] Yang Y, Lin H, Zhang BY, Zhang Y, Zheng X, Yu A, et al. Graphene-based multilayered metamaterials with phototunable architecture for on-chip photonic devices. ACS Photonics. 2019;6(4):1033–40.
[67] Lin H, Sturmberg BC, Lin K-T, Yang Y, Zheng X, Chong TK, et al. A 90-nm-thick graphene metamaterial for strong and extremely broadband absorption of unpolarized light. Nat Photonics. 2019;13(4):270–6.
[68] Lin K-T, Lin H, Yang T, Jia B. Structured graphene metamaterial selective absorbers for high efficiency and

omnidirectional solar thermal energy conversion. Nat Commun. 2020;11(1):1–10.
[69] Bae S, Kim H, Lee Y, Xu X, Park J-S, Zheng Y, et al. Roll-to-roll production of 30-inch graphene films for transparent electrodes. Nat Nanotechnol. 2010;5(8):574.
[70] Wang J, Ma F, Liang W, Wang R, Sun M. Optical, photonic and optoelectronic properties of graphene, h-NB and their hybrid materials. Nanophotonics. 2017;6(5):943.
[71] Phiri J, Gane P, Maloney TC. General overview of graphene: production, properties and application in polymer composites. Mater Sci Engineering: B. 2017;215:9–28.
[72] Wang J, Mu X, Sun M, Mu T. Optoelectronic properties and applications of graphene-based hybrid nanomaterials and van der Waals heterostructures. Appl Mater Today. 2019;16:1–20.
[73] Bao Q, Zhang H, Wang Y, Ni Z, Yan Y, Shen ZX, et al. Atomic-layer graphene as a saturable absorber for ultrafast pulsed lasers. Adv Funct Mater. 2009;19(19):3077–83.
[74] Marini A, Cox J, García de Abajo FJ. Theoretical modelling of the saturable absorption of graphene (Conference Presentation). Strasbourg, France: SPIE Photonics Europe; 2018. doi: 10.1117/12.2306923.
[75] Marini A, Cox J, de Abajo FG, editors. Nonperturbative theory of graphene saturable absorption. European Quantum Electronics Conference. Munich, Germany: Optical Society of America; 2017.
[76] Hasan T, Sun Z, Wang F, Bonaccorso F, Tan PH, Rozhin AG, et al. Nanotube–polymer composites for ultrafast photonics. Adv Mater. 2009;21(38–9):3874–99.
[77] Sun Z, Hasan T, Torrisi F, Popa D, Privitera G, Wang F, et al. Graphene mode-locked ultrafast laser. ACS Nano. 2010;4(2):803–10.
[78] Marini A, de Abajo F. Graphene random laser. arXiv Prepr arXiv. 2015;151204351.
[79] Marini A, Cox J, De Abajo FG. Theory of graphene saturable absorption. Phys Rev B. 2017;95(12):125408.
[80] Gokus T, Nair R, Bonetti A, Bohmler M, Lombardo A, Novoselov K, et al. Making graphene luminescent by oxygen plasma treatment. ACS Nano. 2009;3(12):3963–8.
[81] Ponomarenko LA, Schedin F, Katsnelson MI, Yang R, Hill EW, Novoselov KS, et al. Chaotic Dirac billiard in graphene quantum dots. Science. 2008;320(5874):356–8.
[82] Geng X, Niu L, Xing Z, Song R, Liu G, Sun M, et al. Aqueous-processable noncovalent chemically converted graphene–quantum dot composites for flexible and transparent optoelectronic films. Adv Mater. 2010;22(5):638–42.
[83] Pan D, Zhang J, Li Z, Wu M. Hydrothermal route for cutting graphene sheets into blue-luminescent graphene quantum dots. Adv Mater. 2010;22(6):734–8.
[84] Eda G, Lin YY, Mattevi C, Yamaguchi H, Chen HA, Chen IS, et al. Blue photoluminescence from chemically derived graphene oxide. Adv Mater. 2010;22(4):505–9.
[85] Sun X, Liu Z, Welsher K, Robinson JT, Goodwin A, Zaric S, et al. Nano-graphene oxide for cellular imaging and drug delivery. Nano Res. 2008;1(3):203–12.
[86] Wang J, Cao S, Ding Y, Ma F, Lu W, Sun M. Theoretical investigations of optical origins of fluorescent graphene quantum dots. Sci Rep. 2016;6:24850.
[87] Robertson J, O'reilly E. Electronic and atomic structure of amorphous carbon. Phys Rev B. 1987;35(6):2946.
[88] Kuzmenko A, Van Heumen E, Carbone F, Van Der Marel D. Universal optical conductance of graphite. Phys Rev Lett. 2008;100(11):117401.
[89] Sheats JR, Antoniadis H, Hueschen M, Leonard W, Miller J, Moon R, et al. Organic electroluminescent devices. Science. 1996;273(5277):884–8.
[90] Chien CT, Li SS, Lai WJ, Yeh YC, Chen HA, Chen IS, et al. Tunable photoluminescence from graphene oxide. Angew Commun. 2012;51(27):6662–6.
[91] Liu F, Jang MH, Ha HD, Kim JH, Cho YH, Seo TS. Facile synthetic method for pristine graphene quantum dots and graphene oxide quantum dots: origin of blue and green luminescence. Adv Mater. 2013;25(27):3657–62.
[92] Tsuchiya T, Terabe K, Aono M. *In situ* and non-volatile bandgap tuning of multilayer graphene oxide in an all-solid-state electric double-layer transistor. Adv Mater. 2014;26(7):1087–91.
[93] Tsuchiya T, Tsuruoka T, Terabe K, Aono MJ. *In situ* and non-volatile photoluminescence tuning and nanodomain writing demonstrated by all-solid-state devices based on graphene oxide. ACS Nano. 2015;9(2):2102–10.
[94] Chien CT, Li SS, Lai WJ, Yeh YC, Chen HA, Chen IS, et al. Tunable photoluminescence from graphene oxide. 2012;51(27):6662–6.
[95] Li X, Magnuson CW, Venugopal A, An J, Suk JW, Han B, et al. Graphene films with large domain size by a two-step chemical vapor deposition process. Nano Lett. 2010;10(11):4328–34.
[96] Reina A, Jia X, Ho J, Nezich D, Son H, Bulovic V, et al. Large area, few-layer graphene films on arbitrary substrates by chemical vapor deposition. Nano Lett. 2008;9(1):30–5.
[97] Koma A. New epitaxial growth method for modulated structures using Van der Waals interactions. Surf Sci. 1992;267(1–3):29–33.
[98] Stankovich S, Dikin DA, Dommett GH, Kohlhaas KM, Zimney EJ, Stach EA, et al. Graphene-based composite materials. Nature. 2006;442(7100):282.
[99] Stankovich S, Dikin DA, Piner RD, Kohlhaas KA, Kleinhammes A, Jia Y, et al. Synthesis of graphene-based nanosheets *via* chemical reduction of exfoliated graphite oxide. Carbon. 2007;45(7):1558–65.
[100] Pei S, Cheng H-M. The reduction of graphene oxide. Carbon. 2012;50(9):3210–28.
[101] Hernandez Y, Nicolosi V, Lotya M, Blighe FM, Sun Z, De S, et al. High-yield production of graphene by liquid-phase exfoliation of graphite. Nat Nanotechnol. 2008;3(9):563.
[102] Soldano C, Mahmood A, Dujardin E. Production, properties and potential of graphene. Carbon. 2010;48(8):2127–50.
[103] Novoselov KS, Jiang D, Schedin F, Booth T, Khotkevich V, Morozov S, et al. Two-dimensional atomic crystals. Proc Natl Acad Sci. 2005;102(30):10451–3.
[104] Frazier RM, Daly DT, Swatloski RP, Hathcock KW, South CR. Recent progress in graphene-related nanotechnologies. Recent Pat Nanotechnol. 2009;3(3):164–76.
[105] Worsley KA, Ramesh P, Mandal SK, Niyogi S, Itkis ME, Haddon RC. Soluble graphene derived from graphite fluoride. Chem Phys Lett. 2007;445(1–3):51–6.
[106] Potts JR, Dreyer DR, Bielawski CW, Ruoff RS. Graphene-based polymer nanocomposites. Polymer. 2011;52(1):5–25.

[107] Dhand V, Rhee KY, Kim HJ, Jung DH. A comprehensive review of graphene nanocomposites: research status and trends. J Nanomaterials. 2013;2013:158.
[108] Habiba K, Makarov VI, Weiner BR, Morell G. Fabrication of nanomaterials by pulsed laser synthesis. Manuf Nano. 2014;263–92.
[109] Bhuyan MSA, Uddin MN, Islam MM, Bipasha FA, Hossain SS. Synthesis of graphene. Int Nano Lett. 2016;6(2):65–83.
[110] Yi M, Shen Z. A review on mechanical exfoliation for the scalable production of graphene. J Mater Chem A. 2015;3(22):11700–15.
[111] Zhao G, Wen T, Chen C, Wang X. Synthesis of graphene-based nanomaterials and their application in energy-related and environmental-related areas. Rsc Adv. 2012;2(25):9286–303.
[112] Zhang B, Lee WH, Piner R, Kholmanov I, Wu Y, Li H, et al. Low-temperature chemical vapor deposition growth of graphene from toluene on electropolished copper foils. ACS Nano. 2012;6(3):2471–6.
[113] Li X, Magnuson CW, Venugopal A, Tromp RM, Hannon JB, Vogel EM, et al. Large-area graphene single crystals grown by low-pressure chemical vapor deposition of methane on copper. J Am Chem Soc. 2011;133(9):2816–9.
[114] Guy OJ, Walker K-AD. Chapter 4 – Graphene functionalization for biosensor applications. In: Saddow SE, editor, Silicon carbide biotechnology. 2nd ed. Elsevier; 2016. p. 85–141.
[115] Van Bommel A, Crombeen J, Van Tooren A. LEED and Auger electron observations of the SiC (0001) surface. Surf Sci. 1975;48(2):463–72.
[116] De Heer WA, Berger C, Ruan M, Sprinkle M, Li X, Hu Y, et al. Large area and structured epitaxial graphene produced by confinement-controlled sublimation of silicon carbide. Proc Natl Acad Sci. 2011;108(41):16900–5.
[117] Davis RF, Kelner G, Shur M, Palmour JW, Edmond JA. Thin film deposition and microelectronic and optoelectronic device fabrication and characterization in monocrystalline alpha and beta silicon carbide. Proc IEEE. 1991;79(5):677–701.
[118] Xu Z, Zheng Q-S, Chen G. Elementary building blocks of graphene-nanoribbon-based electronic devices. Appl Phys Lett. 2007;90(22):223115.
[119] Kedzierski J, Hsu P-L, Healey P, Wyatt PW, Keast CL, Sprinkle M, et al. Epitaxial graphene transistors on SiC substrates. IEEE Trans Elect Dev. 2008;55(8):2078–85.
[120] Lin Y-M, Dimitrakopoulos C, Jenkins KA, Farmer DB, Chiu H-Y, Grill A, et al. 100-GHz transistors from wafer-scale epitaxial graphene. Science. 2010;327(5966):662.
[121] Lemme M, Echtermeyer T, Baus M, Kurz H. A graphene field-effect device. IEEE Electron Dev Lett. 2007;28(282):2010.
[122] Liang T, Luan C, Chen H, Xu M. Exploring oxygen in graphene chemical vapor deposition synthesis. Nanoscale. 2017;9(11):3719–35.
[123] Li L. Epitaxial graphene on SiC (0001): more than just honeycombs. In: Sergey M, editor. Physics and applications of graphene-experiments. Rijeka: InTech Europe; 2011. p. 55–72
[124] Raji M, Zari N, el kacem Qaiss A, Bouhfid R. Chapter 1 – Chemical preparation and functionalization techniques of graphene and graphene oxide. In: Jawaid M, Bouhfid R, Qaiss Ae K, editors. Functionalized graphene nanocomposites and their derivatives. Elsevier; 2019. p. 1–20
[125] Xu Y, Bai H, Lu G, Li C, Shi G. Flexible graphene films *via* the filtration of water-soluble noncovalent functionalized graphene sheets. J Am Chem Soc. 2008;130(18):5856–7.
[126] Chang H, Tang L, Wang Y, Jiang J, Li J. Graphene fluorescence resonance energy transfer aptasensor for the thrombin detection. Anal Chem. 2010;82(6):2341–6.
[127] An X, Simmons T, Shah R, Wolfe C, Lewis KM, Washington M, et al. Stable aqueous dispersions of noncovalently functionalized graphene from graphite and their multifunctional high-performance applications. Nano Lett. 2010;10(11):4295–301.
[128] Gupta RK, Malviya M, Verma C, Gupta NK, Quraishi M. Pyridine-based functionalized graphene oxides as a new class of corrosion inhibitors for mild steel: an experimental and DFT approach. RSC Adv. 2017;7(62):39063–74.
[129] Liu J, Fu S, Yuan B, Li Y, Deng Z. Toward a universal "adhesive nanosheet" for the assembly of multiple nanoparticles based on a protein-induced reduction/decoration of graphene oxide. J Am Chem Soc. 2010;132(21):7279–81.
[130] Liu J, Li Y, Li Y, Li J, Deng Z. Noncovalent DNA decorations of graphene oxide and reduced graphene oxide toward water-soluble metal–carbon hybrid nanostructures *via* self-assembly. J Mater Chem. 2010;20(5):900–6.
[131] Xu Y, Liu Z, Zhang X, Wang Y, Tian J, Huang Y, et al. A graphene hybrid material covalently functionalized with porphyrin: synthesis and optical limiting property. Adv Mater. 2009;21(12):1275–9.
[132] Kozhemyakina NV, Englert JM, Yang G, Spiecker E, Schmidt CD, Hauke F, et al. Non-covalent chemistry of graphene: electronic communication with dendronized perylene bisimides. Adv Mater. 2010;22(48):5483–7.
[133] Dong X, Shi Y, Huang W, Chen P, Li LJ. Electrical detection of DNA hybridization with single-base specificity using transistors based on CVD-grown graphene sheets. Adv Mater. 2010;22(14):1649–53.
[134] Chang H, Lv X, Zhang H, Li J. Quantum dots sensitized graphene: *In situ* growth and application in photoelectrochemical cells. Electrochem Commun. 2010;12(3):483–7.
[135] Cao A, Liu Z, Chu S, Wu M, Ye Z, Cai Z, et al. A facile one-step method to produce graphene–CdS quantum dot nanocomposites as promising optoelectronic materials. Adv Mater. 2010;22(1):103–6.
[136] Chang H, Sun Z, Ho KY-F, Tao X, Yan F, Kwok W-M, et al. A highly sensitive ultraviolet sensor based on a facile *in situ* solution-grown ZnO nanorod/graphene heterostructure. Nanoscale. 2011;3(1):258–64.
[137] Zhang H, Lv X, Li Y, Wang Y, Li J. P25-graphene composite as a high performance photocatalyst. ACS Nano. 2010;4(1):380–6.
[138] Li Y, Wang H, Xie L, Liang Y, Hong G, Dai H. $MoS_2$ nanoparticles grown on graphene: an advanced catalyst for the hydrogen evolution reaction. J Am Chem Soc. 2011;133(19):7296–9.
[139] Wang H, Casalongue HS, Liang Y, Dai H. $Ni(OH)_2$ nanoplates grown on graphene as advanced electrochemical pseudocapacitor materials. J Am Chem Soc. 2010;132(21):7472–7.
[140] Liang Y, Li Y, Wang H, Zhou J, Wang J, Regier T, et al. $Co_3O_4$ nanocrystals on graphene as a synergistic catalyst for oxygen reduction reaction. Nat Mater. 2011;10(10):780–6.

[141] Yin Z, Sun S, Salim T, Wu S, Huang X, He Q, et al. Organic photovoltaic devices using highly flexible reduced graphene oxide films as transparent electrodes. ACS Nano. 2010;4(9):5263–8.
[142] Shahid MM, Rameshkumar P, Basirunc WJ, Wijayantha U, Chiu WS, Khiew PS, et al. An electrochemical sensing platform of cobalt oxide@ gold nanocubes interleaved reduced graphene oxide for the selective determination of hydrazine. Electrochim Acta. 2018;259:606–16.
[143] Qi X, Pu KY, Li H, Zhou X, Wu S, Fan QL, et al. Amphiphilic graphene composites. Angew Chem Int Ed. 2010;49(49):9426–9.
[144] Choi E-Y, Han TH, Hong J, Kim JE, Lee SH, Kim HW, et al. Noncovalent functionalization of graphene with end-functional polymers. J Mater Chem. 2010;20(10):1907–12.
[145] Bai H, Xu Y, Zhao L, Li C, Shi G. Non-covalent functionalization of graphene sheets by sulfonated polyaniline. Chem Commun. 2009;13:1667–9.
[146] Bao Q, Zhang H, Yang JX, Wang S, Tang DY, Jose R, et al. Graphene–polymer nanofiber membrane for ultrafast photonics. Adv Funct Mater. 2010;20(5):782–91.
[147] Chang H, Wang G, Yang A, Tao X, Liu X, Shen Y, et al. A transparent, flexible, low-temperature, and solution-processible graphene composite electrode. Adv Funct Mater. 2010;20(17):2893–902.
[148] Zheng W, Shen B, Zhai W. Surface functionalization of graphene with polymers for enhanced properties. In: Gong JR, editor. New Progress on Graphene Research. 2013. doi: 10.5772/50490.
[149] Wang A, Yu W, Fang Y, Song Y, Jia D, Long L, et al. Facile hydrothermal synthesis and optical limiting properties of $TiO_2$-reduced graphene oxide nanocomposites. Carbon. 2015;89:130–41.
[150] Manzano-Ramírez A, López-Naranjo EJ, Soboyejo W, Meas-Vong Y, Vilquin B. A review on the efficiency of graphene-based BHJ organic solar cells. J Nanomater. 2015;406597.
[151] Qin J, Lan L, Chen S, Huang F, Shi H, Chen W, et al. Recent progress in flexible and stretchable organic solar cells. Adv Funct Mater. 2020;30(36):2002529.
[152] Şahin Ç, Diker H, Sygkridou D, Varlikli C, Stathatos E. Enhancing the efficiency of mixed halide mesoporous perovskite solar cells by introducing amine modified graphene oxide buffer layer. Renew Energy. 2020;146:1659–66.
[153] Shi Y, Xing Y, Li Y, Dong Q, Wang K, Du Y, et al. $CH_3NH_3PbI_3$ and $CH_3NH_3PbI_{3-x}$ $Cl_x$ in planar or mesoporous perovskite solar cells: comprehensive insight into the dependence of performance on architecture. 2015;119(28):15868–73.
[154] Huo J, Wu J, Zheng M, Tu Y, Lan Z. High performance sponge-like cobalt sulfide/reduced graphene oxide hybrid counter electrode for dye-sensitized solar cells. J Power Sources. 2015;293:570–6.
[155] Ghasemi S, Hosseini SR, Kazemi Z. Electrophoretic preparation of graphene-iron oxide nanocomposite as an efficient Pt-free counter electrode for dye-sensitized solar cell. J Solid-State Electrochem. 2018;22(1):245–53.
[156] Sasikumar R, Chen T-W, Chen S-M, Rwei S-P, Ramaraj SK. Developing the photovoltaic performance of dye-sensitized solar cells (DSSCs) using a $SnO_2$-doped graphene oxide hybrid nanocomposite as a photo-anode. Opt Mater. 2018;79:345–52.
[157] Lim SP, Pandikumar A, Lim YS, Huang NM, Lim, HN. *In-situ* electrochemically deposited polypyrrole nanoparticles incorporated reduced graphene oxide as an efficient counter electrode for platinum-free dye-sensitized solar cells. Sci Rep. 2014;4:5305.
[158] Le TTN, Le TP, Nguyen TTM, Ho HD, Le KH, Tran MH, et al. Synthesis of zinc oxide/reduced graphene oxide composites for fabrication of anodes in dye-sensitized solar cells. Chem Eng Trans. 2020;78:61–6.
[159] Jayabal P, Gayathri S, Sasirekha V, Mayandi J, Ramakrishnan V. Preparation and characterization of ZnO/graphene nanocomposite for improved photovoltaic performance. J Nanopart Res. 2014;16(11):2640.
[160] Viyada H, Sujinda C, Samuk P, Chatree S, Pornjuk S, Vittaya A. Hierarchical $Fe_3O_4$-reduced graphene oxide nanocomposite grown on NaCl crystals for triiodide reduction in dye-sensitized solar cells. Sci Rep (Nat Publisher Group). 2019;9(1):1–2.
[161] Krishnamoorthy D, Prakasam A. Preparation of $MoS_2$/graphene nanocomposite-based photoanode for dye-sensitized solar cells (DSSCs). Inorg Chem Commun. 2020;118:108016.
[162] Eshlaghi MA, Kowsari E, Ehsani A, Akbari-Adergani B, Hekmati M. Functionalized graphene oxide GO-[imi-$(CH_2)_2$-$NH_2$] as a high efficient material for electrochemical sensing of lead: synthesis surface and electrochemical characterization. J Electroanal Chem. 2020;858:113784.
[163] Wei Q, Sun J, Song P, Yang Z, Wang Q. Synthesis of reduced graphene oxide/$SnO_2$ nanosheets/Au nanoparticles ternary composites with enhanced formaldehyde sensing performance. Phys E: Low-Dimen Syst Nano. 2020;118:113953.
[164] Wang T, Jing L-C, Zhu Q, Ethiraj AS, Tian Y, Zhao H, et al. Fabrication of architectural structured polydopamine-functionalized reduced graphene oxide/carbon nanotube/PEDOT: PSS nanocomposites as flexible transparent electrodes for OLEDs. Appl Surf Sci. 2020;500:143997.
[165] Bano N, Hussain I, El-Naggar A, Albassam A. Reduced graphene oxide nanocomposites for optoelectronics applications. Appl Phys A. 2019;125(3):215.
[166] Son DI, Kwon BW, Park DH, Seo W-S, Yi Y, Angadi B, et al. Emissive ZnO–graphene quantum dots for white-light-emitting diodes. Nat Nanotechnol. 2012;7(7):465–71.
[167] Wang X, Tian H, Mohammad MA, Li C, Wu C, Yang Y, et al. A spectrally tunable all-graphene-based flexible field-effect light-emitting device. Nat Commun. 2015;6(1):1–6.
[168] Lee BR, Kim J-W, Kang D, Lee DW, Ko S-J, Lee HJ, et al. Highly efficient polymer light-emitting diodes using graphene oxide as a hole transport layer. ACS Nano. 2012;6(4):2984–91.
[169] Park M, Nguyen TP, Choi KS, Park J, Ozturk A, Kim SY. $MoS_2$-nanosheet/graphene-oxide composite hole injection layer in organic light-emitting diodes. Electron Mater Lett. 2017;13(4):344–50.
[170] Xu B, Huang J, Ding L, Cai J. Graphene oxide-functionalized long period fiber grating for ultrafast label-free glucose biosensor. Mater Sci Eng: C. 2020;107:110329.
[171] Li P-L, Wang Y-H, Shang M, Wu L-F, Yu X-X. Enhanced optical limiting properties of graphene oxide-ZnS nanoparticles composites. Carbon. 2020;159:1–8.
[172] Chen X, Wang Y, Zhou L, Wang A, Zhang C. Graphene oxide ternary nanohybrids co-functionalized by phenyl porphyrins and thieyl-appended porphyrins for efficient optical limiting. Dye Pigment. 2020;174:108057.

[173] Maharjan S, Liao K-S, Wang AJ, Zhu Z, Alam K, McElhenny BP, et al. Functionalized few-layered graphene oxide embedded in an organosiloxane matrix for applications in optical limiting. Chem Phys Lett. 2019;714:149–55.
[174] Chong MC, Afshar-Imani N, Scheurer F, Cardoso C, Ferretti A, Prezzi D, et al. Bright electroluminescence from single graphene nanoribbon junctions. 2018;18(1):175–81.
[175] Wang X, Tian H, Mohammad MA, Li C, Wu C, Yang Y, et al. A spectrally tunable all-graphene-based flexible field-effect light-emitting device. 2015;6(1):1–6.
[176] Dey AK, Kumar G, Maji PK, Chakrabarty R, Nandi U. Zener-like electrical transport in polyaniline–graphene oxide nanocomposites. RSC Adv. 2020;10(8):4733–44.
[177] Compton OC, Dikin DA, Putz KW, Brinson LC, Nguyen ST. Electrically conductive "alkylated" graphene paper *via* chemical reduction of amine-functionalized graphene oxide paper. Adv Mater. 2010;22(8):892–6.
[178] Chen R, Das SR, Jeong C, Khan MR, Janes DB, Alam MA. Co-percolating graphene-wrapped silver nanowire network for high performance, highly stable, transparent conducting electrodes. Adv Funct Mater. 2013;23(41):5150–8.
[179] Liu Z, Parvez K, Li R, Dong R, Feng X, Müllen K. Transparent conductive electrodes from graphene/PEDOT: PSS hybrid inks for ultrathin organic photodetectors. Adv Mater. 2015;27(4):669–75.
[180] Liu J, Yi Y, Zhou Y, Cai H. Highly stretchable and flexible graphene/ITO hybrid transparent electrode. Nano Res Lett. 2016;11(1):108.
[181] Ahn Y, Jeong Y, Lee D, Lee Y. Copper nanowire–graphene core–shell nanostructure for highly stable transparent conducting electrodes. ACS Nano. 2015;9(3):3125–33.
[182] Hemasiri BWNH, Kim J-K, Lee J-M. Synthesis and characterization of graphene/ITO nanoparticle hybrid transparent conducting electrode. Nano-Micro Lett. 2018;10(1):18.
[183] Lin Z, Liu J, Peng W, Zhu Y, Zhao Y, Jiang K, et al. Highly stable 3D $Ti_3C_2T_x$ MXene-based foam architectures toward high-performance terahertz radiation shielding. ACS Nano. 2020;14(2):2109–17.
[184] Li Z, Wang S-H, Cui J, Wang Y, Zhang J, Xu P, et al. $C_{60}(OH)_{12}$ and its nanocomposite for high-performance lithium storage. ACS Nano. 2020;14(2):1600–8.
[185] Li Q, Zhang Y, Li P, Xue H, Jia N. A nanocomposite prepared from hemin and reduced graphene oxide foam for voltammetric sensing of hydrogen peroxide. Microchim Acta. 2020;187(1):45.
[186] Palanisamy S, Velmurugan S, Yang TC. One-pot sonochemical synthesis of CuS nanoplates decorated partially reduced graphene oxide for biosensing of dopamine neurotransmitter. Ultrason Sonochem. 2020;64:105043.
[187] Liu B, Chen Y, You C, Liu Y, Kong X, Li J, et al. High-performance photodetector based on graphene/$MoS_2$/graphene lateral heterostrurcture with Schottky junctions. J Alloy Compd. 2019;779:140–6.
[188] Liu D, Li H-J, Gao J, Zhao S, Zhu Y, Wang P, et al. High-performance ultraviolet photodetector based on graphene quantum dots decorated ZnO nanorods/GaN film isotype heterojunctions. Nano Res Lett. 2018;13(1):261.
[189] Yadav A, Upadhyaya A, Gupta SK, Verma AS, Negi CMS. Poly-(3-hexylthiophene)/graphene composite based organic photodetectors: the influence of graphene insertion. Thin Solid Films. 2019;675:128–35.
[190] De Fazio D, Goykhman I, Yoon D, Bruna M, Eiden A, Milana S, et al. High responsivity, large-area graphene/$MoS_2$ flexible photodetectors. ACS Nano. 2016;10(9):8252–62.
[191] Zhang D, Jing F, Gao F, Shen L, Sun D, Zhou J, et al. Enhanced performance of a $TiO_2$ ultraviolet detector modified with graphene oxide. RSC Adv. 2015;5(102):83795–800.